Characterising Silicon Diode Response for Radiation Measurements

BY

Nyakodzwe Walter

A THESIS SUBMITTED IN PARTIAL FULFILMENT OF THE REQUIREMENTS FOR THE DEGREE OF MASTER OF SCIENCE IN APPLIED PHYSICS

DEPARTMENT OF PHYSICS
FACULTY OF SCIENCE
UNIVERSITY OF ZIMBABWE

December 2011

Acknowledgement

I am deeply grateful to my academic supervisor, Dr. L Olumekor for the guidance and encouragement throughout the project.

I am deeply grateful to the professional and dedicated staff of the University of Zimbabwe Physics Department, for providing the foundation of knowledge necessary.

I am also deeply grateful to the entire staff at Parirenyatwa Hospital Radiotherapy Center for their guidance and contribution to my preparation for entering into the medical physics profession. Special thanks go to Mr. Mhatiwa, Mr. Dzangare, Dr T.A Erlwanger and Mr. Mukwada for their valuable guidance and support.

I am grateful to the following Mr Mhukayesango, Ms Nhiwatiwa, Ms Tapera and the Nyakodzwe family for their encouragement.

Finally I would like to thank Germany Academic Exchange Services (DAAD) for the scholarship award.

Dedication

To my parents with love

Table of Contents

List of Figures

List of Tables

Abstract

X-ray radiation has been used in the treatment of cancer since its discovery in 1895. It was found that incorrect use of x-radiation can cause irreversible damage. It was necessary to introduce diode in-vivo dosimetry for x-radiation measurement to control the dose administered to patients.

This study focuses on the characteristics of a p-type silicon diode as an x-radiation detector. The investigation involved measurement of the response of the diode under different conditions, which include gantry angle, field size, source to surface distance, off axis and wedge angle, in order to determine the optimum position for diode placement for both flat and curved surface.

These conditions were varied and the corresponding change in response of the diode noted. The measurements were done on both the flat and curved surface of a phantom designed and built specifically for this project. Two diodes (old diode and new diode) were used in the investigation to observe the change in diode sensitivity after prolonged use. The results were also compared to those of other workers [8,10,15,20,23].

The results showed that the old and new diode both exhibited similar trends in all measurements though notable difference in their sensitivity can be observed. Large percentage deviations about ± 7 % were observed in the curved surface measurements. The diodes responded differently between the curved and flat surface measurements. The project showed that proper diode placement is necessary especially when performing measurements on curved surfaces.

Chapter 1

INTRODUCTION

1.1 Background

X-rays are used in the treatment of cancer and has proved to be very effective in treatment and diagnosis of some diseases. High energy x-radiation is produced by a linear accelerator commonly called a Linac. Linacs produce both high energy x-rays (photons) and high energy electrons, which are used in the treatment of superficial tumours.

High energy photons are produced by the interaction between electrons travelling with almost the speed of light and a target material. The target material is normally a high atomic number element such as copper or tungsten. The electrons are used in treatment when the target material is retracted from the path of the electrons and they are allowed to hit a scattering foil to create a beam.

X-ray treatment has also proved to be very fatal if applied incorrectly, hence the need to have a method of accurately measuring and determining the dose delivered to a point in tissue. Several methods and instruments were developed for dose determination. The methods include the use of ionisation chamber, films, thermoluminescence dosimeters, MOSFETs and diodes.

The diode in-vivo dosimetry has been used as an effective tool for quality assurance in radiotherapy. The diodes have been widely received by many radiotherapy centers and have been recommended by many professional bodies. The physics of charge generation at the p-n junction of a silicon semiconductor help in understanding how absorbed dose can be measured.

The p-n junction of a diode is used to measure the amount of radiation absorbed at a point. This method of directly inferring the amount of energy deposited per unit mass in tissue is known as in-vivo dosimetry. In-vivo dosimetry is used clinically as a tool for comprehensive quality assurance.

The ability to accurately measure the amount of energy absorbed is of immense importance, since the accuracy in the absorbed dose to the tumour of 5% is required to obtain total tumour control [1,5]. Proper diode placement is necessary to achieve accurate measurements during clinical use. Ideal diode placement is not always possible hence the need to establish the relationship between diode placement and measured dose accuracy. Measurements performed on a flat surface often are different from those obtained on a tilted surface. The sensitivity variation of the diode may be affected by several parameters including temperature, accumulated dose and distance from the x-radiation source. The response of the diode is also affected by beam modifiers also called wedges, which are defined as any device capable of attenuating an x-radiation beam thereby modifying its property.

Calibration of diodes is performed so that the charge generated by radiation is directly converted to the absorbed dose. The use of correction factors help to reduce the errors caused as a result of the difference between the calibration conditions and the measurement conditions. Measurement conditions are similar to those shown in figure 1.1 while calibration conditions are as shown in figure 1.2.

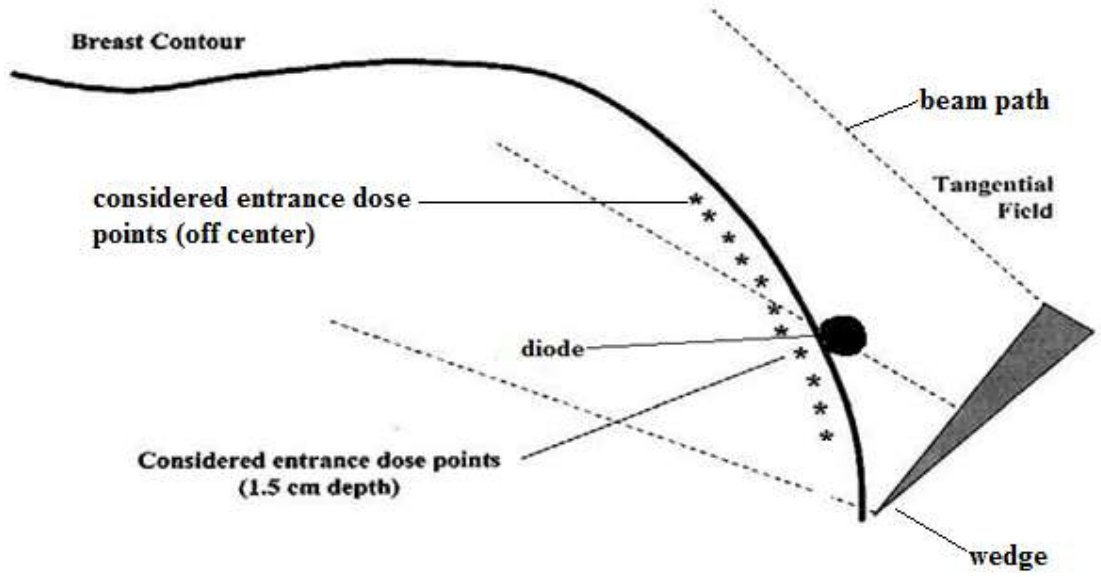

Figure 1.1: An illustration of a definition of incidence angle, and typical locations of points (indicated with asterisks) where entrance dose is to be determined [20].

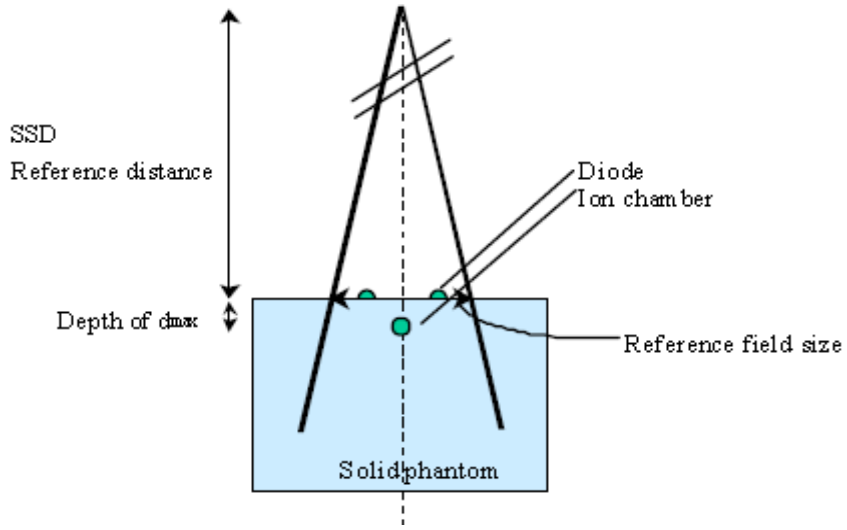

Figure 1.2: Diode calibration procedure for dose measurements. The ionisation chamber is positioned at the reference depth in the phantom and the diode at the entrance [4]

Gas filled ionisation chambers are instruments used to detect and measure radiation. Ionisation chambers did not become popular for in-vivo dosimetry because they require an external bias, are less sensitive and are generally bulky as compared to the semiconductor

diode. Semiconductor diodes have the following advantages which makes them favourable for in-vivo dosimetry, high sensitivity, fast response time, small size, absence of external bias, good mechanical stability, excellent reproducibility and prompt dose inference. Thermoluminescence dosimeters (TLDs) and MOSFETs are also used for dose measurements in many departments and they have been a subject of many researches [21, 22, 24, 25].

The diodes used for in-vivo dosimetry can either be p-type or n-type. The choice of diode depends on the department but several literatures highlight the fact that p-type are better than n-type [8], this is because p-type have a lower instantaneous dose rate dependence.

Integrating an in-vivo dosimetry system into the quality assurance programme of a department safeguards the patients from serious errors as well as machine malfunctions. AAPM-TG 40 [18] recommends that clinics should use an in-vivo system to avoid misadministration of dose to patients.

1.2 Statement of the problem

Most investigations for in-vivo dosimetry using diodes were done for detectors placed on a flat surface with the central axis of the beam perpendicular to the diode. Deviations of ±15% are encountered when performing in-vivo dosimetry, due to inaccurate detector placement especially under conditions of oblique incidence and in the presence of wedges. Diode placement under conditions different from calibration conditions, affects the sensitivity of the radiation detector, hence the need to investigate the response characteristics of a silicon diode as a radiation detector under these conditions.

1.3 Significance of Study

The project seeks to address the problem of large uncertainties caused by diode placement which are not within the calibration conditions. Notable causes include field size, distance from the x-ray source, wedges and diode placement which changes from patient to patient. The study will investigate how these parameters, when combined, can affect practical clinical action levels achievable. It will also address the effect of diode positioning and the angle of beam incidence relative to the diode. A number of experiments will be conducted on a phantom with similar properties to that of human tissue and air spaces present in the thorax region of a human body.

The knowledge gathered during this study will be of immense value to diode manufacturers and users in hospitals. This study will also provide a better understanding of the performance of diodes used in clinics.

1.4 Objectives

The objectives of this study are:

a) To review the current calibration procedures of the diodes used in in-vivo dosimetry.
b) To build and evaluate a measurement phantom using local resources.
c) To measure the response of the diode under the physical conditions of field size, gantry angle, distance from central axis and wedge angle on both flat and curved surface.
d) To observe the significance of the diode response of the old diode against the new diode.

1.5 Study Outline

The study is divided into six chapters. The first chapter introduces the topic and gives a brief background on the subject of investigation. Chapter 2 gives literature review related to the study, and it compares some results obtained by other researchers. Chapter 3 focuses on the experimental techniques and methods used to obtain the results given in chapter 4. Chapter 5 follows with the discussion and analysis of the results. Then finally chapter 6 gives a brief summary of results, conclusions and recommendations.

Chapter 2

LITERATURE REVIEW

2.1 Introduction

This chapter gives an overview of the underlying physics principles involved in radiation measurements. The chapter gives an insight into the basic radiation physics followed by the process of x-ray production. The interactions of radiation with matter together with dose calculation and quantification methods are also addressed in this chapter. Types of radiation measurement devices and their principles of operation are also given with major emphasis on the diodes. The chapter concludes with a review of the results from other researchers.

2.2 Basic radiation physics

Radiation is basically grouped into two classes which are:

a) ionising radiation; and
b) non ionising radiation.

Ionising radiation is radiation which ionises matter either directly or indirectly. Directly ionising radiation includes electrons, protons, α particles and heavy ions and indirectly ionising radiation includes photons, γ rays and neutrons.

The directly ionising radiation deposits energy in the medium through direct coulomb interaction between the ionising charged particles and orbital electrons of the medium. During indirect ionisation two processes occur; charged particles are released in the medium (i.e. photons release electrons or positrons and neutrons release protons). The released

charged particles then deposit energy in the medium as in the case of direct ionisation [19]. Both the direct and indirect ionising radiation are used in radiation treatment.

The type of ionising radiation produced is mostly dependent on the type of machine involved e.g γ rays from a cobalt machine, x-rays and electrons from a Linac. The machines were developed over a period of years starting from orthovoltage machine through particle accelerators to Linacs, whose development took more than 40 years [19].

2.3 Production of x-radiation

Linear accelerators (Linacs) accelerate electrons to kinetic energies between 2 and 25 MeV. It uses non conservative microwaves radio frequency (rf) fields in the frequency range from 10^3 MHz (L band) to 10^4 MHz (X band) [6,19]. The Linac used in this project operates specifically at 2856 MHz (S band).

The electrons are accelerated following straight trajectories in special evacuated structures called accelerating waveguides. The electrons assume a linear path through the waveguide.

The high power rf fields used for electron acceleration in the accelerating waveguide are produced through a process of decelerating electrons in the retarding potential in several evacuated devices called magnetrons and klystrons.

The accelerated high energy electrons then emerge from the exit window of the accelerator (figure 2.1). The electrons assume the shape of a pencil beam with a diameter of about 3 mm [6].

In a low energy Linac (6 MV) the accelerated electrons are allowed to proceed straight and strike a target for x-ray production. While in higher energy (10-18 MV) machines, the

electrons are bent through a suitable angle between the accelerator and target to produce x-rays as shown in figure 2.1. The ionising radiation produced then interacts either directly or indirectly with matter as described in section 2.2.

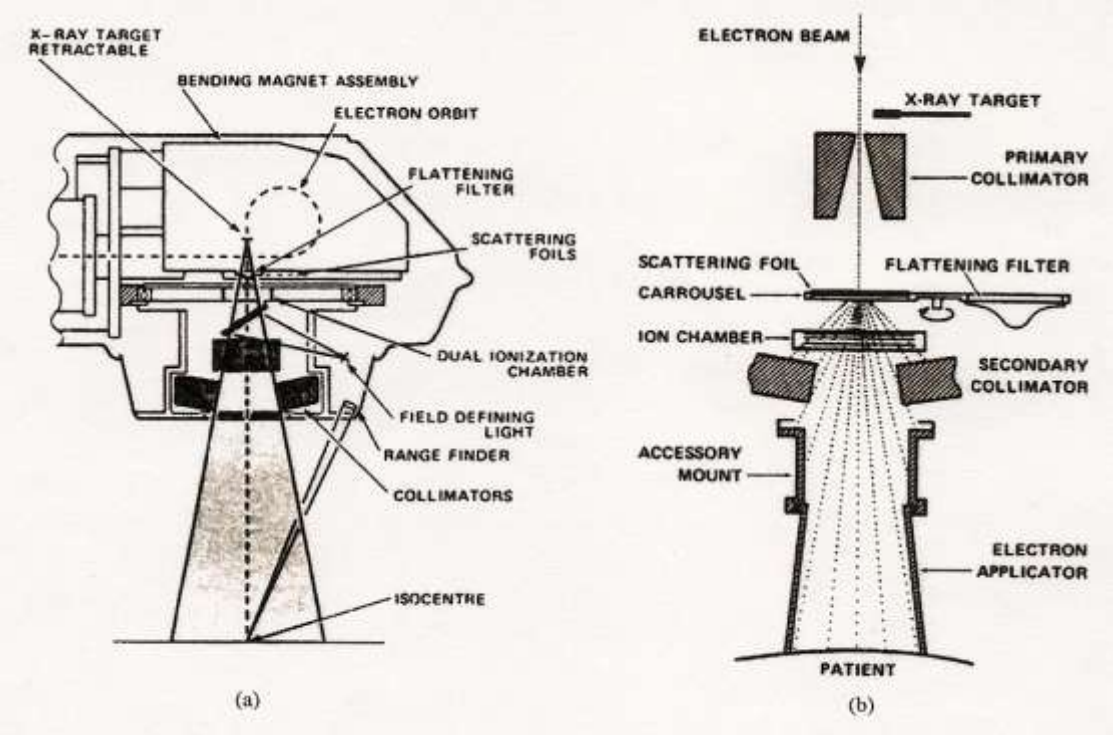

Figure 2.1: Schematic diagram of the treatment head of a linear accelerator [6]

2.4 Interaction of radiation with matter

Biological damage occurs when a radiation beam passes into an absorbing medium such as body tissue. A fraction of the energy carried by the beam is transferred to the medium. The energy deposited per unit mass of the medium is called the absorbed dose. The absorbed dose can also be referred to as a quantity for predicting biological effects [14]. The remaining fraction of the energy of the x-ray beam is radiated from the absorber as scattered radiation.

The collective interaction or attenuation of radiation with the absorber can be represented by:

$$I(x) = I_0 e^{-\mu x} \quad 2.1$$

where x is the thickness of the absorber, $I(x)$ and I_0 are the instantaneous and incident beam intensities respectively and μ is the linear attenuation coefficient and it characterises the broad beam interaction with matter.

μ is defined as the fraction of photons attenuated per unit thickness of material and is a function of photon energy and the atomic number of the medium [6]. The linear attenuation values indicate the rate at which photons interact as they move through material and are inversely related to the average distance photons travel before interacting.

The radiation interaction (attenuation, scattering, and absorption) in matter result in the need for quantification of absorbed dose, following this several quantities and units were developed from first principles.

2.5 Radiation quantities and units

The interaction of radiation with matter is dependent on the nature of radiation (i.e. radiation type and energy) and matter (i.e. atomic number and density). The measurement of radiation and its effects involve measurement of radiometric and dosimetric quantities.

Radiometric quantities describe the properties of a radiation beam. Beam properties are described by particle fluence, Φ and energy fluence, ψ. Particle fluence is defined as the number of particles (dN) crossing an area (da) taken at right angles to the direction of the radiation beam [14]. The unit for particle fluence is the number of particles per unit area. Podgorsak [19] and Khan [6] went further to define the energy fluency, ψ as the amount of energy (dE) crossing an area (da). Mathematically, it is given by:

$$\Psi = \frac{dE}{da} \qquad 2.2$$

Dosimetric quantities determine radiation energy transfer and its deposition in matter as a result of the interaction processes. The fundamental dosimetric quantities used in radiation dosimetry are kerma and absorbed dose.

Kerma is defined as the kinetic energy released per unit mass in the medium [6]. The dose equivalent is defined as the product of the absorbed dose, *(D)* and the quality factor, *(Q)*. The quality factor refers to the biological effectiveness of the type of radiation. The SI unit of absorbed dose is the Gray (Gy).

The absorbed dose can be obtained through mathematical calculations using several parameters which were found to affect the distribution of dose in matter. The parameters include field size, depth dose variation, source to surface distance (SSD) and energy.

2.6 Dose calculation

Several methods are available for calculating absorbed dose in a medium. Two methods commonly used are the source to surface distance (SSD) and the source to axis distance (SAD). The two have their advantages and disadvantages relative to each other.

2.6.1 The SSD method

In this method, the percentage depth dose (PDD) is used in the calculation of monitor units (MU) utilised in delivering the required dose. The PDD is defined according to Khan [6], as the absorbed dose at any depth, *d* to the absorbed dose at a reference depth, d_{max} along the central axis of the beam.

$$PDD = \frac{TD \times 100}{D_{max}}, \quad 2.3$$

where *TD* is the absorbed dose at depth, *d* and D_{max} is the dose at a reference depth.

The monitor unit is defined as the time during which a particular amount of dose is delivered to a point. The high energy x-ray machines are calibrated to deliver 1 cGy/MU at a reference depth of d_{max} for a reference field size of 10 cm x 10 cm (see Appendix II). The monitor unit necessary to deliver a target dose, *(TD)* at a depth, *d* for a field size *r* at the surface at SSD = 100 cm are given by:

$$MU = \frac{TD \times 100}{K \times PDD \times S_c(r) \times S_p(r) \times (SSD\ Factor)}, \quad 2.4$$

where *k* = 0.01 Gy/MU, *r* is the collimator field size, S_c is a factor related to field size at source axis distance, *(SAD)* and S_p is a factor related to the field treating the patient.

In this study it is necessary to measure the maximum dose for calculated monitor units. The maximum dose will be measured by the diodes. The theoretical maximum dose can be obtained by using the definition of PDD given in equation 2.3 and rearranging it gives the following equation:

$$D_{max} = \frac{TD \times 100}{PDD}. \quad 2.5$$

2.6.2 The SAD method

In this method, also known as the isocentric method, the tissue maximum ratio *(TMR)* is used for the dosimetric calculation. The *MU* necessary to deliver isocenter dose, *(ID)* at depth, *d* is given by:

$$MU = \frac{ID}{K \times TMR(d, r_d) \times S_c(r) \times S_p(r) \times (SAD\ Factor)}, \quad 2.6$$

$$TMR(d, 0) = e^{-\mu(d - t_0)}, \quad 2.7$$

where μ is the effective linear attenuation coefficient and t_0 is the reference depth of maximum dose, and

$$SAD\ factor = \left(\frac{SCD}{SAD}\right)^2, \quad 2.8$$

where *SCD* is the chamber source to chamber distance. The calculated doses can be complemented by direct measurement using irradiation measurement instruments.

2.7 Radiation measurement devices

The radiation measurement devices also called dosimeters are instruments or systems that measure or evaluate either directly or indirectly the quantities highlighted in section 2.5, which include kerma, absorbed dose and dose equivalence.

Solid state dosimetry is the area of focus of this project though there are several other types of dosimeters available commercially. The solid state detectors can only be used as relative dosimeters because they need to be calibrated against a known standard for them to be used effectively.

2.7.1 Solid state devices

There are two types of solid state dosimeters:

a) Integrating type dosimeters (thermoluminescent crystals, radiophoto-luminescent glass, optical density type dosimeters such as glass and film); and
b) Electrical conductivity dosimeters (semiconductor junction detectors, induced conductivity in insulating material).

Films, thermoluminescent dosimeters (TLDs) and diodes are commonly used.

2.7.2 Silicon diode

Silicon p-n junction diodes are used for dosimetry and have been used as radiation detectors for over 30 years [7,8]. The physics of charge generation and collection in silicon semiconductor diodes provide characteristic features, which make them useful as radiation detectors. A cross section of a 6 MV Isorad Sun Nuclear diode used in radiation measurement is shown in figure 2.2.

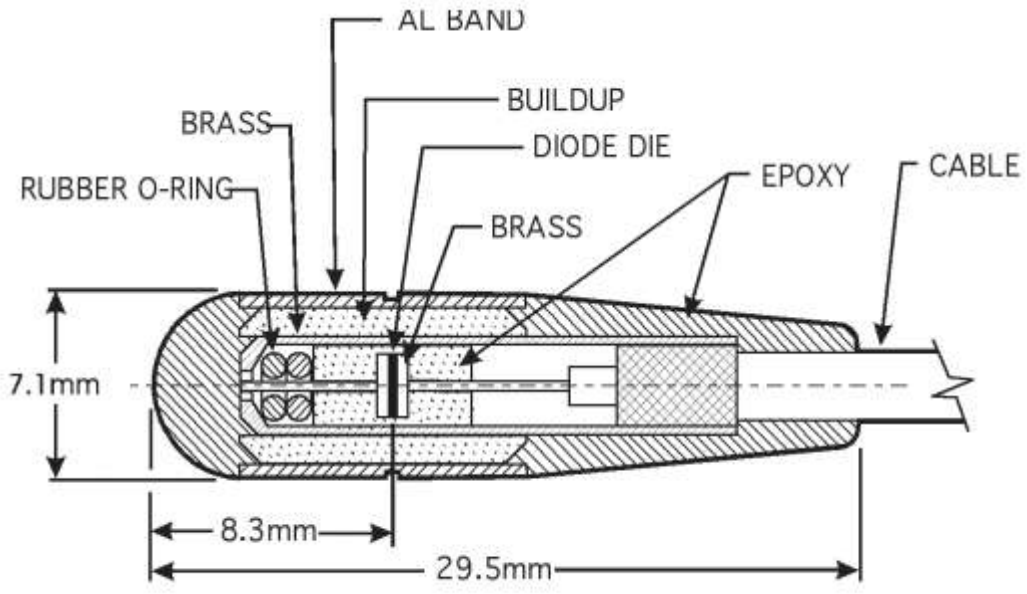

Figure 2.2: Cross sectional view of a diode used for in-vivo dosimetry [10]

The silicon die with an active detection thickness of 15 μm [10] is the location of electron hole pair generation caused by radiation. York *et al* [8] describes the process of charge generation and measurement as the following:

a) Primary or secondary particles from the radiation source are absorbed thus generating electron hole pairs throughout the diode.
b) The electrons and holes generated within one diffusion length from the junction are able to reach the p-n junction.
c) The excess minority carriers (electrons on the p side and holes on the n side) are swept to the opposite sides of the build-in potential across the p-n junction giving rise to a pulse in the external circuit.
d) When the diode terminals are connected to the input of an operational amplifier, the charges generated by the irradiation are collected, amplified, measured and converted to dose.

Diode detector sensitivity, S is approximately proportional to the minority carrier diffusion length, L and is given by:

$$S = aL = a\sqrt{\tau D}\,, \qquad 2.9$$

where a = constant, τ = lifetime of radiation generated excess carriers, and D = minority carrier diffusion coefficient.

The change in sensitivity of the diode affects the accuracy of the measurements hence the need for correction factors. Most investigations [2-4,7,9,11,12] for diode in-vivo dosimetry were done for detectors placed on a flat surface.

2.8 Theory of Silicon diodes

Silicon diodes have very small dimensions hence the sensitivity relative to the ionisation volume is high [13, 17]. The sensitive volume is small and well defined, the effective point of measurement can be placed less than 1 mm below the outer surface of the detector. Recent silicon detectors are surrounded by water equivalent material and special care is exercised to optimise their performance in radiation dosimetry to reduce the interface phenomena.

The electrical properties (conductivity) of a semiconductor material can be changed by introducing impurities into the crystal also called doping.

The n-type silicon is obtained by doping silicon with Group V (P, As, or Sb) elements called donors and p-type silicon by doping with Group III (B, Al, Ga, or In) elements called acceptors. The p-type silicon is joined with an n-type material to obtain a p-n junction.

2.8.1 P-N junction

A p-n junction is an internal boundary between the p-type and n-type regions in a single crystal. The n-type material has a large concentration of electrons and few holes, while the p-type material has a large concentration of holes and few electrons. When these two regions are joined together, diffusion of charge carriers takes place because of the large gradient of carrier concentration at the junction. Electrons in the n side diffuse to the p side, and holes in the p side diffuse to the n side due to the gradient. Holes diffusing from p region leave uncompensated acceptors while electrons diffusing from n to p region leaves behind uncompensated donor ions in the n region.

There is positive space charge near the n side, and negative space charge near the p side of the material. The charged ions left on both sides form a depletion region (space charge) over which a built-in voltage drop of about 0.7 V is created over a distance of few micrometers

[4,8 ,10,13]. The p-n junction is formed when equilibrium is reached. There is no net current flow across the junction at equilibrium until it is irradiated. During irradiation electron-hole pairs are created as described in section 2.7.2 from (a) to (d). The current signal is due to charge carriers created in the depleted region and the minority carriers created in the base material that diffuse to the depletion region.

The thickness of the effective volume is determined by the lifetime of the carrier and is due to recombination centres and traps in the crystal. The traps consist of imperfection in the crystal lattice. Rickener and Grusell [13] identified and described the following:

a) type of doping;
b) doping level;
c) pre-irradiation level;
d) mechanical construction;
e) detector volume;
f) leakage current and connection to the connector, as parameters which also influence the behaviour of the detectors.

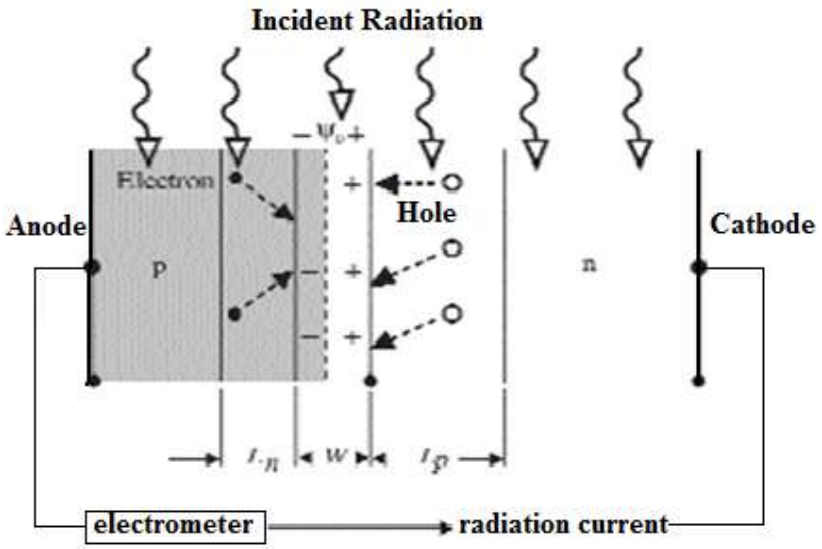

Figure 2.3: Schematics of a silicon p-n junction diode as a radiation detector.

A pictorial summary of the recombination process is as shown in figure 2.4.

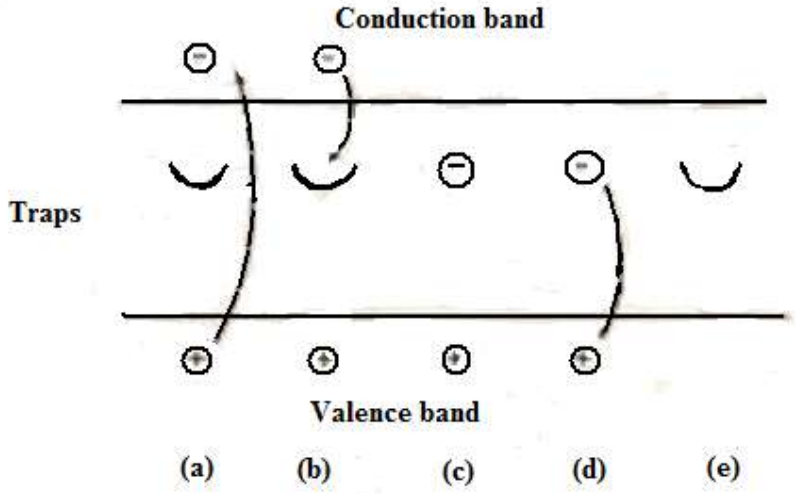

Figure 2.4: Recombination by traps in p-type silicon. When irradiated, electron–hole pairs are created. Minority carriers will move in the conduction band (a) until they are trapped (b) and occupy the traps (c) before they recombine with majority carriers (d). In (e) recombination is complete.

2.9 Recombination-generation centers

In gas filled ion chambers direct ion recombination is the major process and this reduces the amount of charge collection as the ion density increases. This is different when semiconductor silicon diodes are involved. Radiation-generated electron-hole (e-h) pairs recombine indirectly through the energy levels in the energy gap between the conduction and valence band of silicon as shown in figure 2.4. The energy levels are formed by the defects and impurities in silicon and they are called recombination-generation centers because they capture and emit carriers.

The recombination-generation (r-g) centers act as intermediaries in the direct recombination process. The empty r-g centers first capture minority carriers. The captured carrier will remain trapped until the trapping center captures a majority carrier resulting in recombination.

When the diode is irradiated most of the excess minority carriers within one diffusion length are swept across the p-n junction and are collected. A small portion of them are captured by the r-g centers and are recombined. The captured portion of minority carriers depends on the following:

a) The excess carrier concentration;
b) The empty trapping centers concentration; and
c) The capture cross section of the minority carriers.

The radiation interrupts the equilibrium of the p-n junction and thus the net recombination rates do not disappear under steady state conditions. The net steady state recombination for a single energy level trapping center is given by:

$$R = \frac{np - n_i^2}{\tau_p(n + n_1) + \tau_n(p + p_1)}, \qquad 2.10$$

where $n = \Delta n + n_o$ and $p = \Delta p + p_o$ are the electron and hole concentration respectively, n_o, p_o are the equilibrium electron and hole concentration, n_i is the intrinsic carrier concentration of the material.

n_1 and p_1 are computable constants. $\tau_p and\ \tau_n$ are minority carrier life time.

For electrons and holes in the p-type and n-type respectively $n_0\ and\ p_0$ can be obtained from the following expressions:

$$n_0 = n_i e^{\frac{(E_F - E_i)}{KT}} \quad \text{and} \qquad 2.11$$

$$p_0 = p_i e^{\frac{(E_i - E_F)}{KT}} . \qquad 2.12$$

The trapping centers are responsible for the diodes' instantaneous dose rate dependency, sensitivity variation with accumulated dose, sensitivity variation with temperature and sensitivity variation with SSD.

2.10 Diode factors calculation methods

The diode calibration factor F_{cal} can be calculated from:

$$F_{cal} = D_w \left(\frac{100 + d_{max}}{R(100)}\right) , \qquad 2.13$$

where D_w $(100 + d_{max})$ is the dose to water or the ionisation chamber reading at (100+d_{max}) cm SSD and $R(100)$ is the diode reading at 100 cm SSD.

The general equations utilised for obtaining the corrected dose is given by:

$$D_{corr}(X_1 \dots X_{n1}, x_1 \dots x_{n2}) = \left(\prod_{i=1}^{n2}(k)(x)_i \prod_{j=1}^{n1} C_j X_j\right) F_{cal} R(X_1 \dots X_{n1}, x_1 \dots x_{n2}), \qquad 2.14$$

where R is the original diode reading under the particular conditions from the electrometer. The beam and phantom correction factors are denoted by $C_j X_j$. Intrinsic response correction factors are given by $(k)(x)_i$.

For intrinsic correction factors, K_i

$$K_\theta = \frac{R(\theta=0)}{R(\theta)} \quad , \qquad 2.15$$

where θ, is the angle between the beam axis and the detector.

A correction factor is a dimensionless multiplier used to correct measurement results obtained under non standard conditions. It is calculated using equation 2.15, where the numerator is taken as the measurement result under standard conditions and the denominator is the measurement result under non standard conditions.

2.11 Review of previous work

Several investigations about characterising diodes for clinical use were done by many hospitals. Sun Nuclear Corporation also did an independent check on the response of their diodes during clinical trials. The investigations were limited to flat water equivalent material, hence the study was done on plastic water phantoms as given in figure 1.2.

The following graphs illustrate the results of the work performed by others including the manufacturers in trying to characterise the response of the diode under different conditions. The results below are for different types of diodes not necessarily the p-type Isorad diode, but they give a trend we should expect under different conditions.

Figures 2.5 and 2.6 gives the work by Colussi [23] and the Sun Nuclear Corp [10] respectively, on the response of the cylindrical diodes variation with change in beam angle incidence.

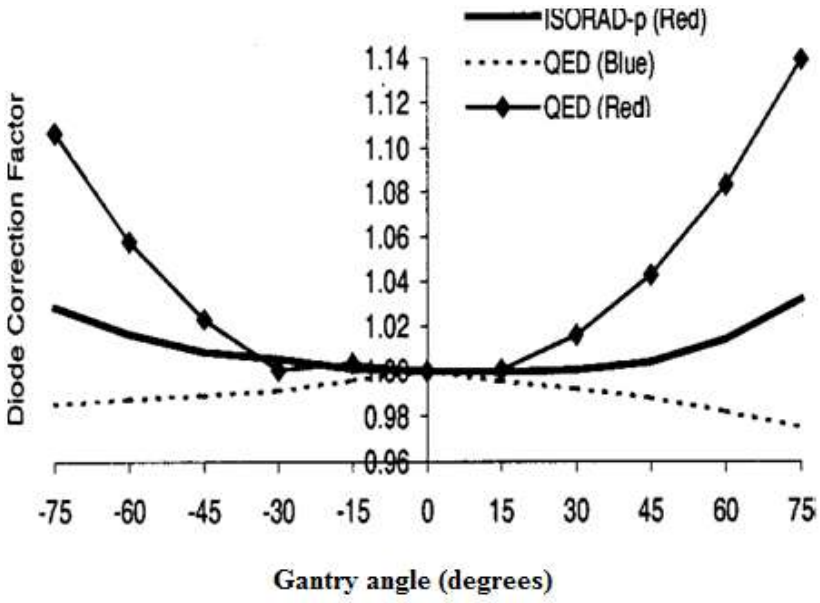

Figure 2.5: Diode angular correction factors [23].

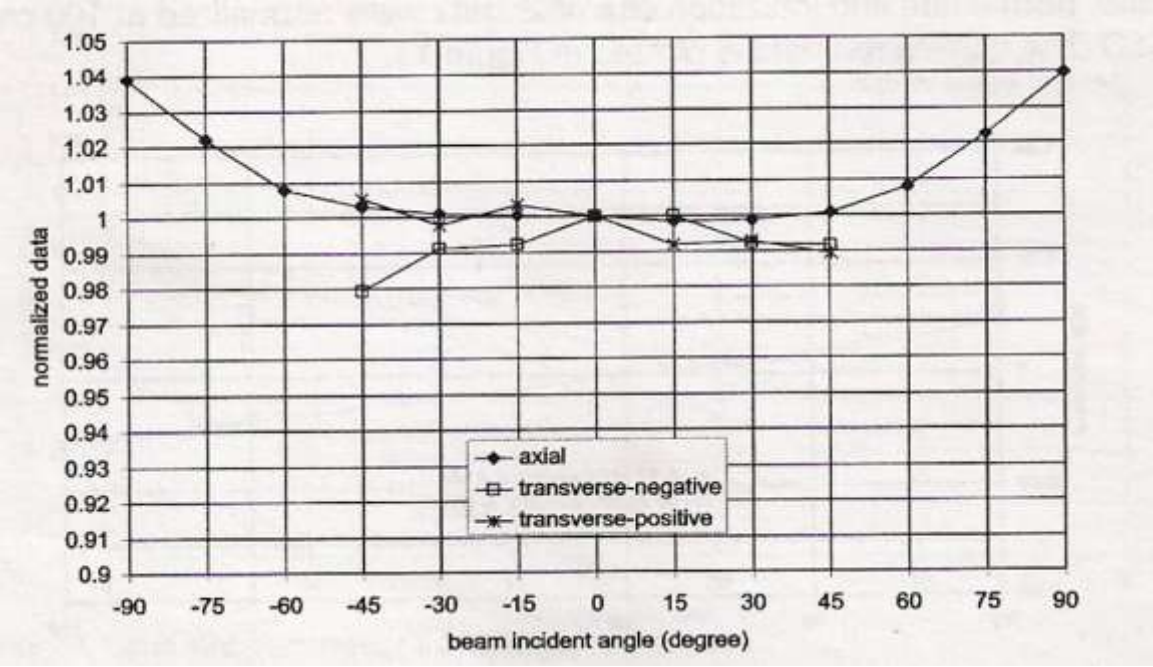

Figure 2.6: Directional response of detector measured at 6 MV photon beam [10].

The following figures 2.7, 2.8 and 2.9 show how the diode responds to change in field size.

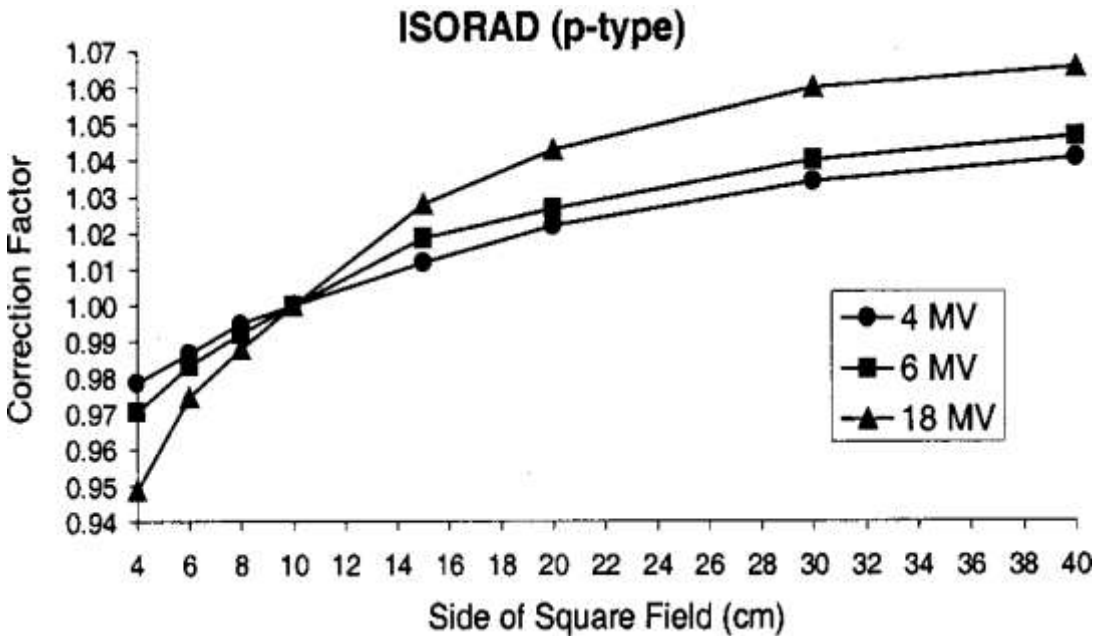

Figure 2.7: ISORAD p-type diode open field size correction factors for 4, 6 and 18 MV photon beams for 100 SSD [23].

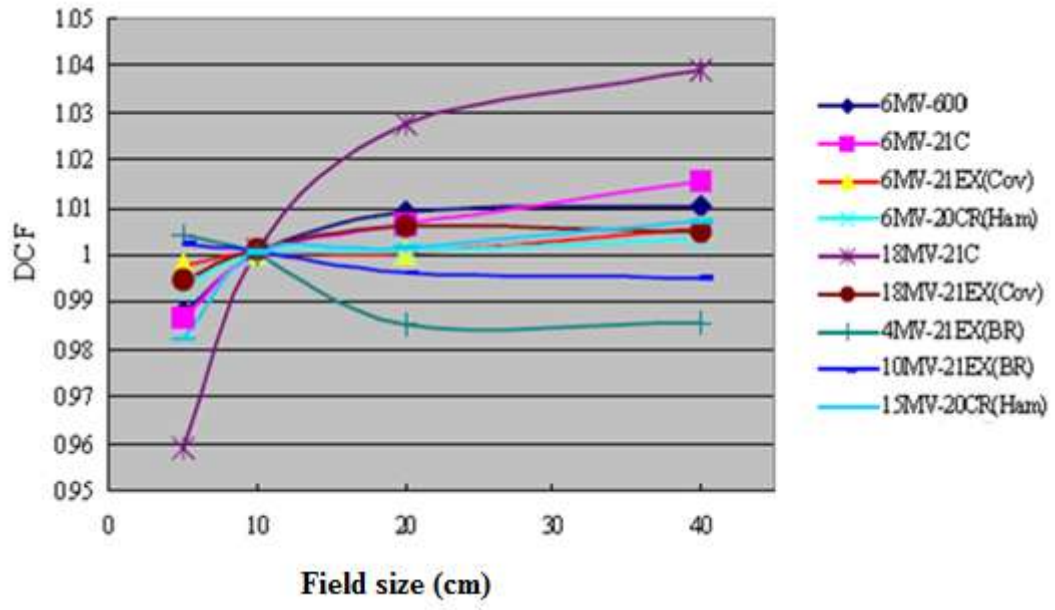

Figure 2.8: Diode correction factor as a function of field size (open fields) [15].

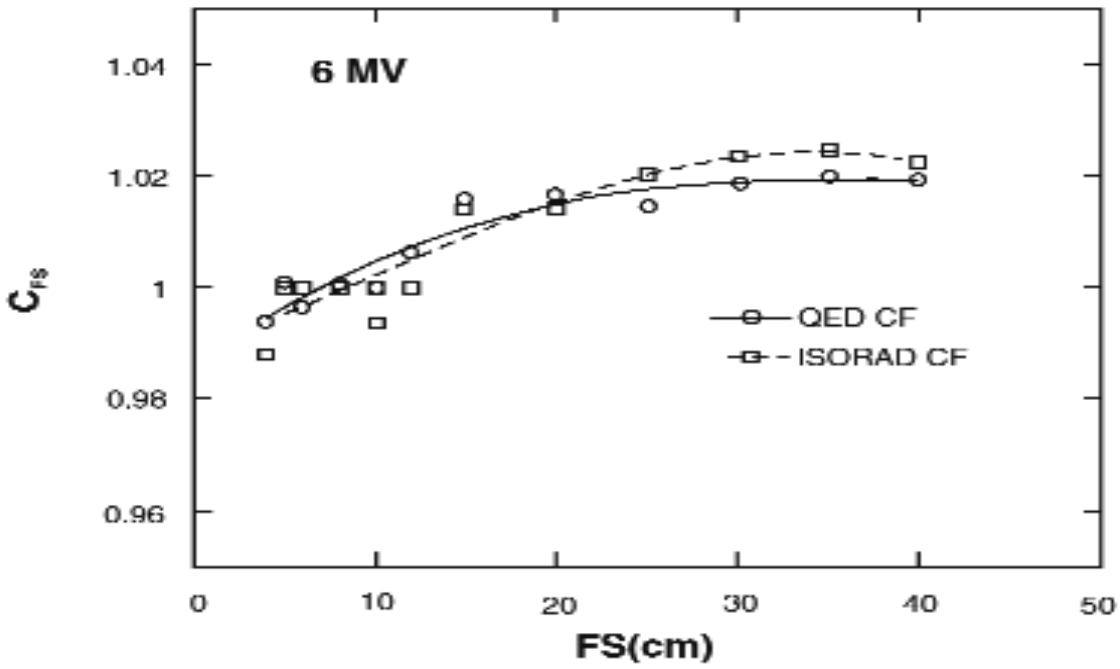

Figure 2.9: Diode correction factor as a function of field size in a 6 MV photon beam [8].

Figures 2.10 and 2.11 shows the work by Huang [15] and Yorke *et al* [8] respectively, on the response of the diode with change in source to surface distance (SSD).

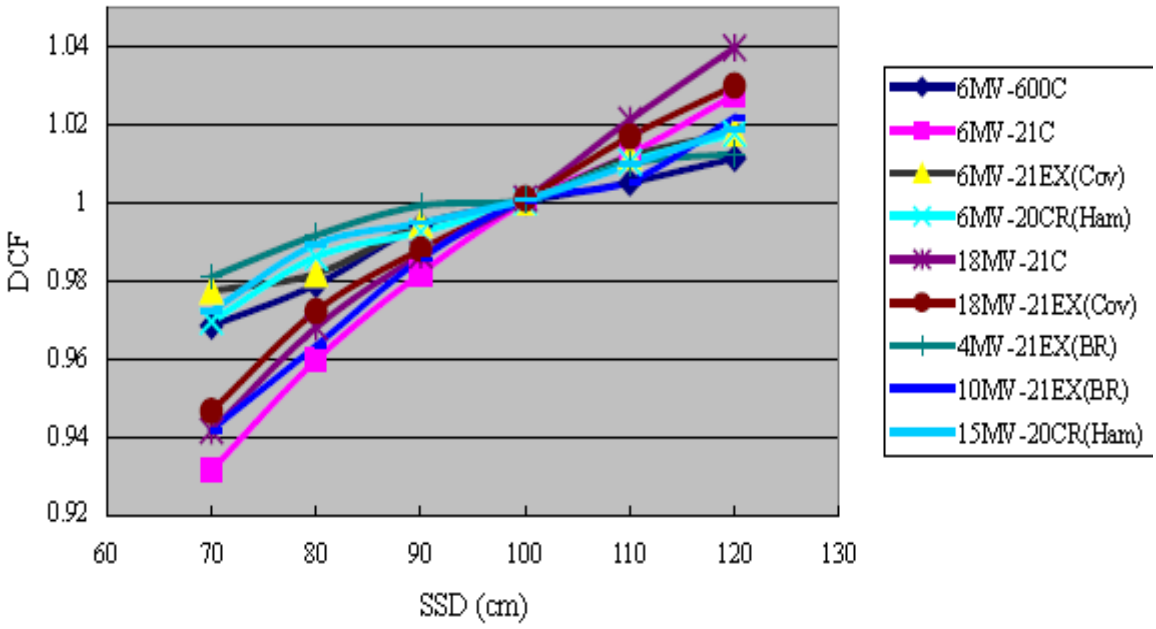

Figure 2.10: Diode correction factors as a function of source to surface distance (SSD) [15].

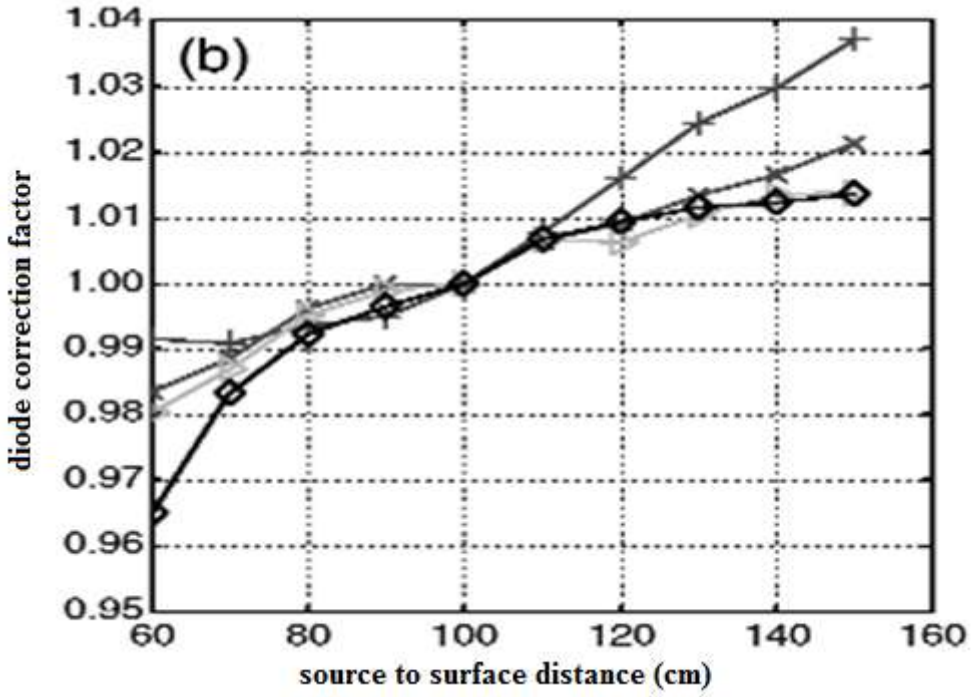

Figure 2.11: SDD correction factors for diodes measured at the surface in a full scatter phantom under different types of diodes [8].

Figure 2.12 shows the work by Herbert *et al* [20] on the variation of the diode response as the diode is moved away from the central axis (off-axis)

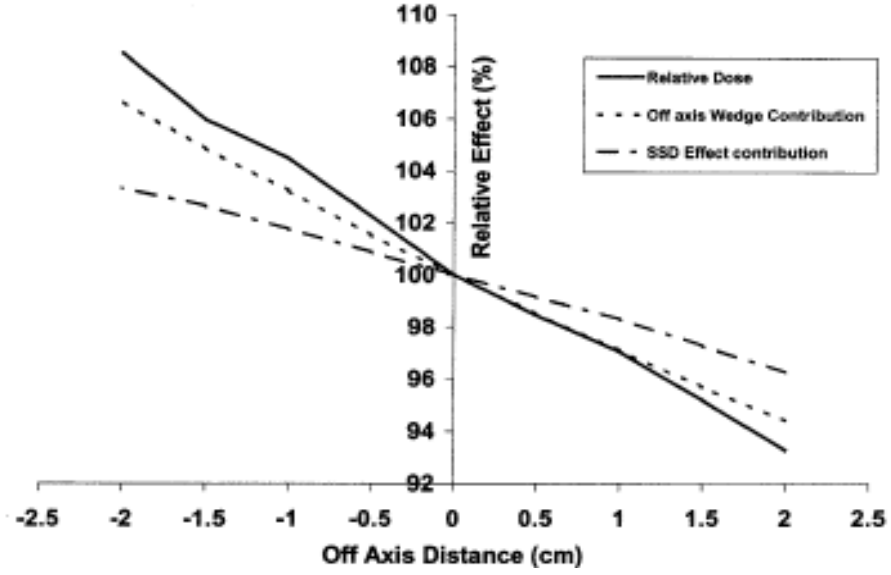

Figure 2.12: SSD and off axis wedge contribution to the variation of the relative entrance dose [20].

The major difference between this work and the work from other authors[8,10,15,20,23], is the use of the phantom for measurements. The phantom has similar properites to that of an actual patient. The phantom is expected to offer different scatter contribution to the measured dose, hence the measured dose will be different from that of the water equivalent material. This is as result of the different properties between the two phantoms .

The phantom is most ideal for correction factor measurements involving the thorax region, which is composed of areas with some air spaces and the curved surface.

The principle of conservation of energy can be applied here to quantify the extent of the scattered radiation contribution.

The incident radiation should be the sum of the absorbed radiation and the scattered radiation. This principle can help us to deduce the extent of the scattered contribution due to the difference in the type of phantom used.

The work done by other researchers did not address all clinical situations for example curved surfaces and the need to consider different densities of materials. This project will address this and reduce percentage deviations observed for curved surface measurements.

Chapter 3

MATERIALS AND METHOD

3.1 Introduction

This chapter deals with the methodology of the project. The work is divided into two parts:

i) Calibration of the diodes used in the project; and

ii) The measurement procedures and manufacturing of phantom.

The first part involves reviewing the current calibration procedures for diodes and making recommendations about the possible improvements in diode calibration. The second part involves all the measurement procedures, starting with the building of a phantom and testing its applicability with respect to tissue-density similarity with that of an actual patient. The second part also involves the actual measurement processes thus identifying the parameters of concern.

A comparison of the obtained results with existing data from other researchers and from the manufacturer will be done.

3.2 Calibration of the diode

The manufacturer of the p-type Isorad diodes (Sun Nuclear Corporation) including other authors [4,8] set detailed calibration procedures for the diodes. The calibration procedures are similar in that they use an ionisation chamber as a reference to obtain the required calibration factors as outlined in section 2.10.

The diodes should be calibrated first before clinical use to convert the charge generated into absorbed dose. The calibration of a diode to measure the entrance dose is generally done in two steps;

a) The dose on the central axis is determined using a calibrated ionisation chamber at d_{max}, which is defined as the depth of maximum dose in a plastic phantom with similar properties to that of water and using the IAEA TRS 277 (Appendix II) protocol to obtain the absorbed dose per monitor unit at d_{max}. Daily calibration of the machine using TRS 277 protocol ensures that 1cGy/MU is delivered at d_{max}.

b) The diode is fixed on the top of the phantom using the same setup as in calibration, just as it will be taped to the patient's skin (figure 1.1). The internal build-up in the diode detector should be sufficient to provide electronic equilibrium for the energy being measured. The centre of the detecting volume of the diode should be aligned with the central axis of the beam. The diode is irradiated with the same intensity as that used for the ion chamber.

The calibration factor is obtained by finding the ratio of the ion chamber reading (step a) to the diode reading (step b) as given by equation 2.10. This is done automatically by the in-vivo dosimetry equipment, the system calculates the calibration factor and stores it.

After these two steps the diode is ready to measure the dose at d_{max}. Validation of the diodes is necessary before daily use to keep track of the possible damage to the diodes caused by radiation and prolonged use.

3.3 Validation of diodes

The TG 40 document from the American Association of Physicist in Medicine (AAPM) on comprehensive quality assurance in radiotherapy [18] recommends that the calibration procedure and its results be documented and recorded.

The validating procedure involves a repeat of the calibration procedures and comparing the obtained results with the documented results. The percentage deviation should not be greater than ±2% otherwise recalibration would be necessary.

3.4 Choice of diodes

Two Isorad p-type diodes (Sun Nuclear Corporation) with negative output were chosen. The first diode was an old diode calibrated for clinical use in 2007, while the second diode was a new diode which was specifically for this project. The old diode with serial number 5320617 was validated using the initial dose and calibration conditions to ensure that it was still measuring dose accurately.

The new diode with serial number 5216919 was calibrated using the procedures in section 3.2, the two diodes were used under the same conditions for comparison.

3.5 Building of the phantom

The materials used for the construction of the phantom include:

a) 5 styrofoam blocks measuring 30 x 30 x 4 cm^3;
b) Contact glue;
c) Cutting tool;

d) 1.5 cm bolus; and

e) Plaster of Paris for outline moulding.

The building process was as follows:

A patient was used to obtain an outline of the body contour using plaster of paris. The blocks of styrofoam were fused together using contact glue forming a cube measuring approximately 10 cm width, 30 cm length and 20 cm height. The height of the volume was used as the length of the body phantom. The contour obtained from the patient was transferred onto the joint styrofoam using ink. The pattern was cut using a cutting tool into a volume similar to that of a human thorax as shown in figure 3.1. A bolus of tissue equivalent material was then applied as a top layer which represented the skin as shown in figure 3.2.

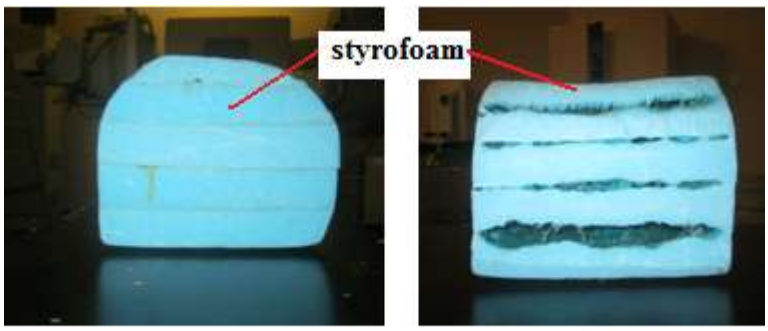

Figure 3.1: A volume of styrofoam fused and cut into the shape of the thorax region, (a) front view of the phantom and (b) side view of phantom.

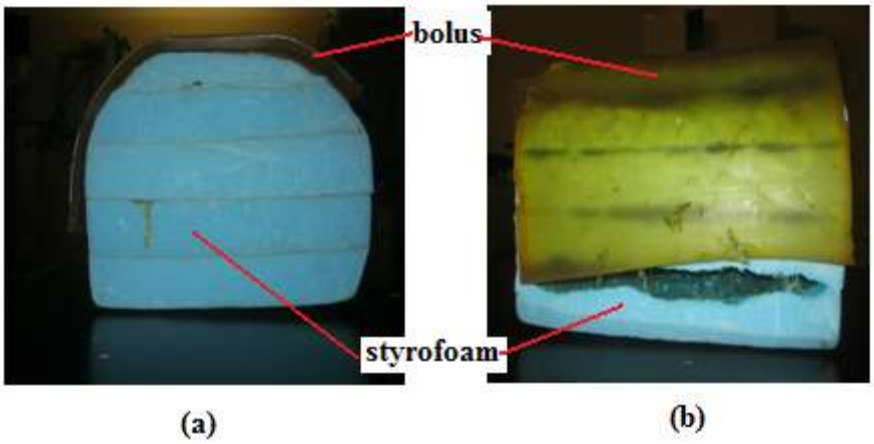

Figure 3.2: A volume of styrofoam cut into the shape of the thorax region with bolus, (a) front view of the phantom and (b) side view of phantom.

The reason why styrofoam was used was because it has the similar electron density to that of air to represent the thorax region of the body. The electron density of the body phantom was verified by taking computerised tomography (CT) scan slices of the phantom and comparing them with that of the CT scan of the chest of a patient.

3.6 Limitations

A single block of styrofoam with the required dimensions to produce a half body phantom was not readily available in the department. Therefore, a styrofoam with the required dimensions was obtained using contact glue. The glue etched the styrofoam in some areas thereby creating air spaces though the phantom remained intact. The glue and styrofoam made an interface which may have an effect on the accuracy of the measurement result, this was confirmed by the CT slices obtained as shown in figure 3.3.

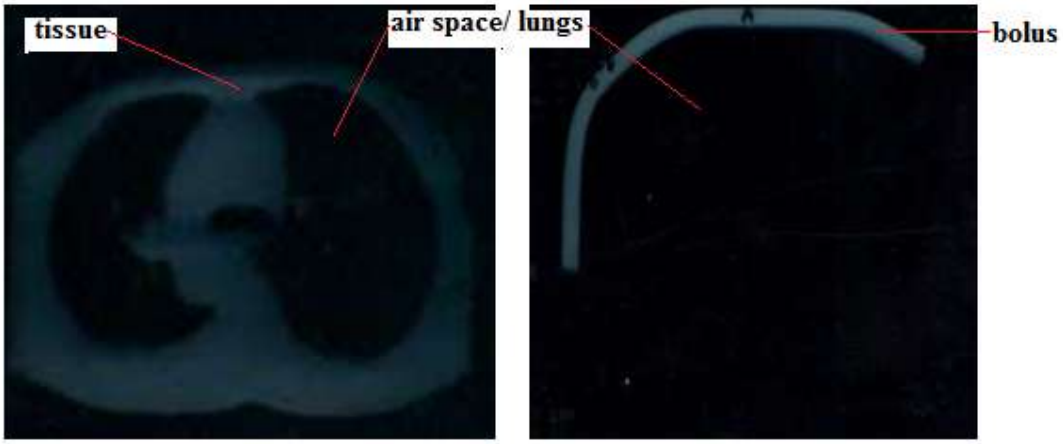

Figure 3.3: Comparison of patient and phantom using Computerised Tomography images.

3.7 Measurement procedures

After the phantom was built successfully, a comparison with an actual CT scan for the upper body region was done. The phantom was used for measurements since radiation measurements could not be done on actual patients. The diodes were assigned names new diode (ND) and old diode (OD) respectively. The measurements were done in two phases which are:

a) on flat surface of the phantom; and

b) on curved surface of the phantom.

The ND and the OD were both used in the measurements, so that a comparison of the two diodes could be achieved. The response of the diodes was measured as a function of the following:

a) Gantry angle;

b) Field size;

c) Source to surface distance (SSD);

d) Distance from the central axis; and

e) Wedge angle.

The methods of measurements for (a) to (e) are given in sections 3.7.1 to 3.7.5.

3.7.1 Gantry Angle

The phantom was laid on the treatment couch and positioned as a patient would have been positioned without the breast board. A diode was placed transversely (with respect to the axis of rotation of the gantry) on the central part of the phantom and aligned using a sagital laser as shown in figure 3.4.

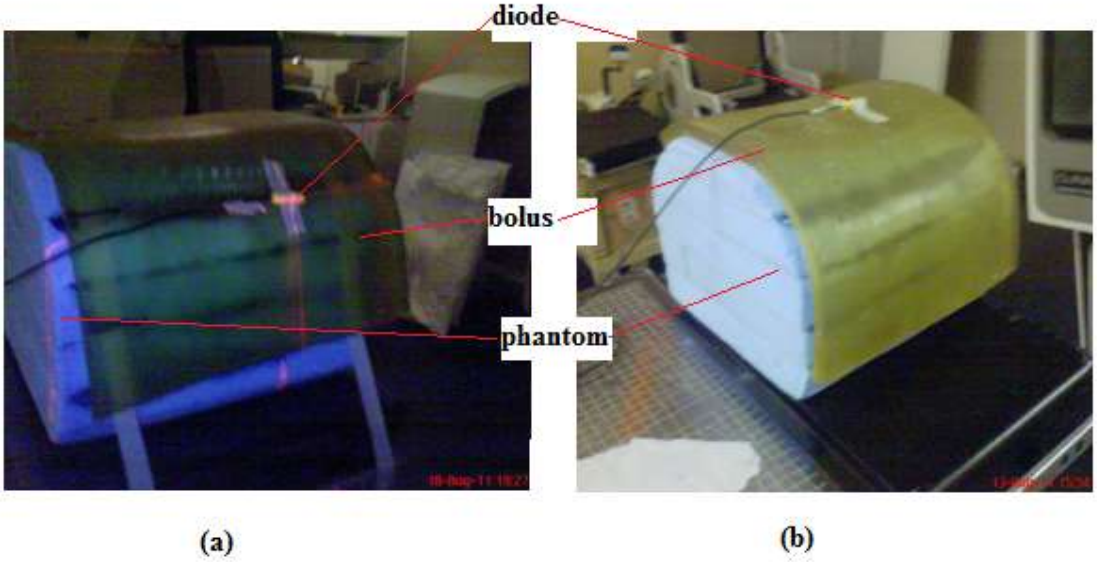

Figure 3.4: Diode setup and positioning on phantom for, (a) diode placed on curved surface, and (b) diode placed on the flat surface

The gantry was set to 0° and this was taken as the nominal position. An arbitrary field size of 5 cm x 10 cm was used at a distance of 100 cm from the x-ray source. A dose of 100 cGy was delivered to the phantom at 3 cm depth such that a dose at d_{max} was measured. The two diodes (OD and ND) were irradiated using 109 MU at 0° gantry angle, the measured readings were collected and recorded. The irradiations were repeated for gantry angles ranging from 70° in the counter clockwise direction to 290°, the gantry angles from 0° to 290° were taken as negative. The gantry can rotate through 360° about a point called the isocenter.

The second phase of the measurements was done with the setup exactly as for flat surface measurement, except that the diode was placed transversely on the most curved part of the phantom as shown in figure 3.4. The two calibrated diodes were irradiated at 0° gantry angle, the measured readings were recorded. The irradiations were repeated for gantry angles ranging from 120° to 310°, with the gantry angles from 0° to 310° taken as negative. This range of angles was the most ideal for curved surface measurements.

3.7.2 Field size

The diode response for different field sizes was investigated by varying the respective field sizes, and noting the corresponding changes in response of the diode. The two diodes were also used for the procedure. The effects of using rectangular fields having the same equivalent square field values were also investigated.

The diode was placed at 100 cm from the x-ray source on the phantom as shown in figure 3.4. A dose of 100 cGy was delivered to a depth of 3 cm using rectangular fields whose equivalent field size was calculated. The field sizes were varied and the response of the diode was noted for both the rectangular field and the equivalent square field (which is basically a

square field). A comparison of the correction factor for the rectangular field and the corresponding equivalent square field was done. These two types of field sizes are taken to be equal in dosimetry and hence should have the same correction factors and the same response characteristics.

3.7.3 Source to surface distance (SSD dependence)

Measurements were only performed on the flat part of the phantom. Field sizes of 5 x 5 cm^2, 10 x 10 cm^2, and 20 x 20 cm^2 were used for the two diodes. For each field size the distance from the source to the surface of the phantom was varied from 80 cm to 120 cm and calculations to deliver 100 cGy to a depth of 3 cm for the respective SSD and field sizes was made.

The response of the diode for the varying SSD was noted and a comparison of the trend of the response for different field sizes was made.

3.7.4 Off-axis diode dependence

Off-axis distance is any distance measured away from the central axis, thus the off-axis dose simply refers to the dose measured away from the central axis. The profile of the dose varies from machine to machine and is highly dependent on the type and shape of the flattening filters in the machine figure 2.1.

The measuring point of a radiation beam in radiotherapy is on the central axis. The dose is defined at this point and the measuring optical distance indicator is expected to be linear along the central axis. The diode response when moving away from the central axis (off-axis)

is expected to be the same as the central axis response if the beam is flat but is expected to vary with a change in SSD.

A field size of 10 x 10 cm^2 was set on the machine and the phantom was placed at 100 cm SSD. Measurements were done with the diode placed on both the curved surface and the flat surface. The doses were measured for the range -4 cm to 4 cm from the central axis, the negative represents the distance measured from the central axis towards the left, while the positive represent the opposite.

A dose of 100 cGy at 3 cm depth was administered and the doses at points away from the central axis were measured and the corresponding correction factors obtained. The new diode and the old diode were both used in the investigation. The experiment was repeated with the diode placed at points off-axis on the curved surface of the phantom and results were recorded and compared with those of flat surface.

3.7.5 Wedge angle dependence

A wedge as shown in figure 1.1 is a device which modifies the x-ray beam intensity profile by attenuation, thereby modifying its shape. The wedge affects the dose rate dependence of a diode.

The phantom was positioned as in figure 3.4. Four types of physical wedges were selected for the experiments. There were 15°, 30°, 45° and 60° wedges. Larger field sizes of 20 x 20 cm^2 could not be used during measurement using the 60° wedge.

An arbitrary dose of 100 cGy was delivered to the phantom at 3 cm depth at a constant SSD of 100 cm.

Table 3.1 gives the possible combination of field sizes and wedge angles used in the measurements. In all cases the same dose was delivered to the phantom at 3 cm depth.

Table 3.1: Possible combination between field size and wedge angle

Field Size (cm^2)	Wedge angles used
5	15º, 30º, 45º, 60º
8	15º, 30º, 45º, 60º
10	15º, 30º, 45º, 60º
12	15º, 30º, 45º, 60º
15	15º, 30º, 45º, 60º
20	15º, 30º, 45º

Chapter 4

RESULTS AND DISCUSSION

4.1 Introduction

This chapter presents the results of the measurements for the diode response characteristics with different parameters. The methods of obtaining the results are clearly given in chapter 3. The results are shown as tables and graphs. The graphs show the variation of the diode correction factors and dose with the investigated parameters namely gantry angle, field size, SSD, off-axis and wedge angle.

The results obtained from the validation process are also given in this chapter. A selected number of measurements were done both for phase 1 and phase 2. Phase 1 was for the measurements obtained for a flat phantom surface and phase 2 is for the curved surface measurements.

This chapter also presents the discussion of results obtained in light of the objective of the study, literature review and the experimental techniques outlined in chapters 1, 2 and 3 respectively. The results are given first, followed by a discussion of the results so that it is easy to follow the work.

4.2 Validation

Table 4.1: Results for the validation of the old diode.

N^{th} Reading	Electrometer Reading (cGy)
1	101.8
2	102.0
3	101.9
4	102.1
5	102.2
6	102.0

From Table 4.1, it is noticed there are N = 6 observations therefore,

$\bar{x} = 102.0$ cGy, 4.1

where $\bar{x}$ is the average reading. The deviation of each measurement from the mean is calculated and the sum of the squares is obtained to give the result in equation 4.2;

$$\sum_1^N (x_n - \bar{x})^2 = 0.1 \quad 4.2$$

Using equation 4.3, the standard deviation can be obtained,

$$\sigma = \sqrt{\frac{\sum_1^N (x_n - \bar{x})^2}{N-1}}, \quad 4.3$$

which is simplified to obtain,

$$\sigma = 0.1414$$

The standard error from mean (SEM) α is calculated using equation 4.4

$$\alpha = \sqrt{\frac{\sum_1^N (x_n - \bar{x})^2}{N(N-1)}}, \quad 4.4$$

which becomes;

$$\alpha = 0.06$$

Therefore the measured dose from the diode becomes 102.00 ± 0.06 cGy

4.3 Angular dependence

Table 4.2: Results for variation of measured dose and diode correction factor with gantry angle, obtained for the central flat surface of the phantom.

Gantry Angle (°)	Measured Dose ND (cGy)	Measured Dose OD (cGy)	Correction Factor (ND)	Correction Factor (OD)	± % deviation (ND)	± % deviation (OD)
-70	106.5	105.9	1.0009	1.0144	0.09	1.44
-60	105.9	104.9	0.9953	1.0048	0.47	0.48
-50	105.8		0.9944	1.0019	0.56	0.19
-40	105.7	104.4	0.9934	1.0000	0.66	0.00
-30	105.7	104.3	0.9934	0.9990	0.66	0.10
-20	105.8	104.3	0.9944	0.9990	0.56	0.10
-10	105.9	104.4	0.9953	1.0000	0.47	0.00
0	106.4	104.4	1.0000	1.0000	0.00	0.00
10	106.2	104.6	0.9981	1.0019	0.19	0.19
20	106	104.6	0.9962	1.0019	0.38	0.19
30	106.1	104.8	0.9972	1.0038	0.28	0.38
40	106.2	104.1	0.9981	0.9971	0.19	0.29
50	106.2	104.9	0.9981	1.0048	0.19	0.48
60	106.4	105.5	1.0000	1.0105	0.00	1.05
70	106.6	105.8	1.0019	1.0134	0.19	1.34

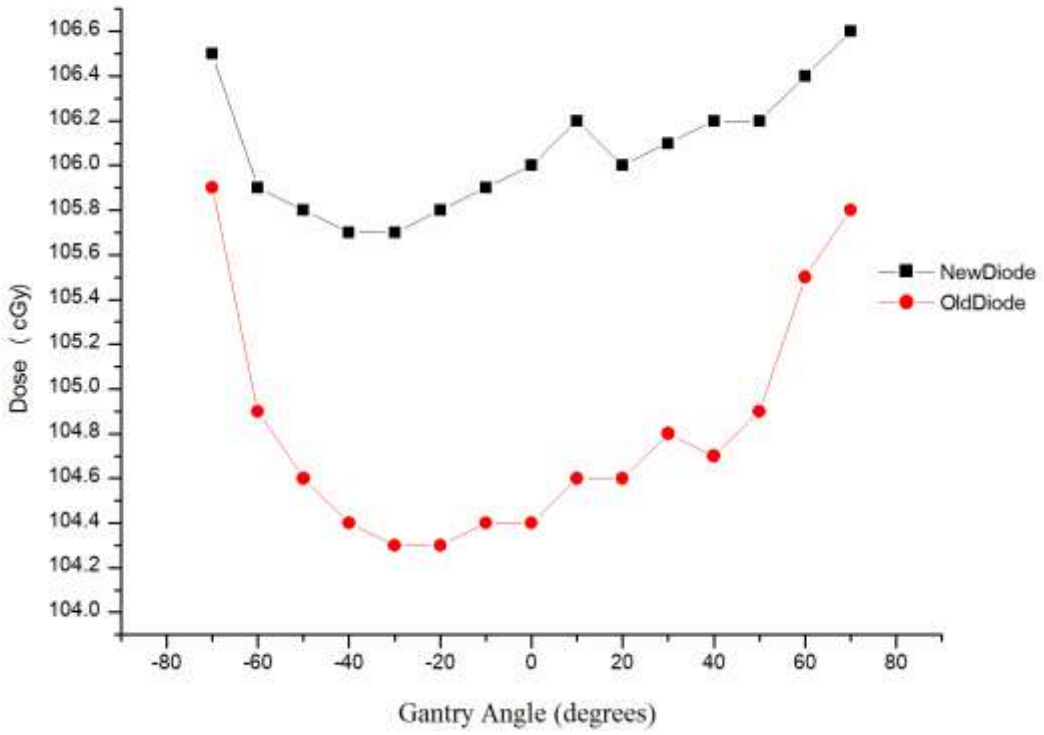

Figure 4.1: Variation of the measured dose as a function of gantry angle on a flat surface.

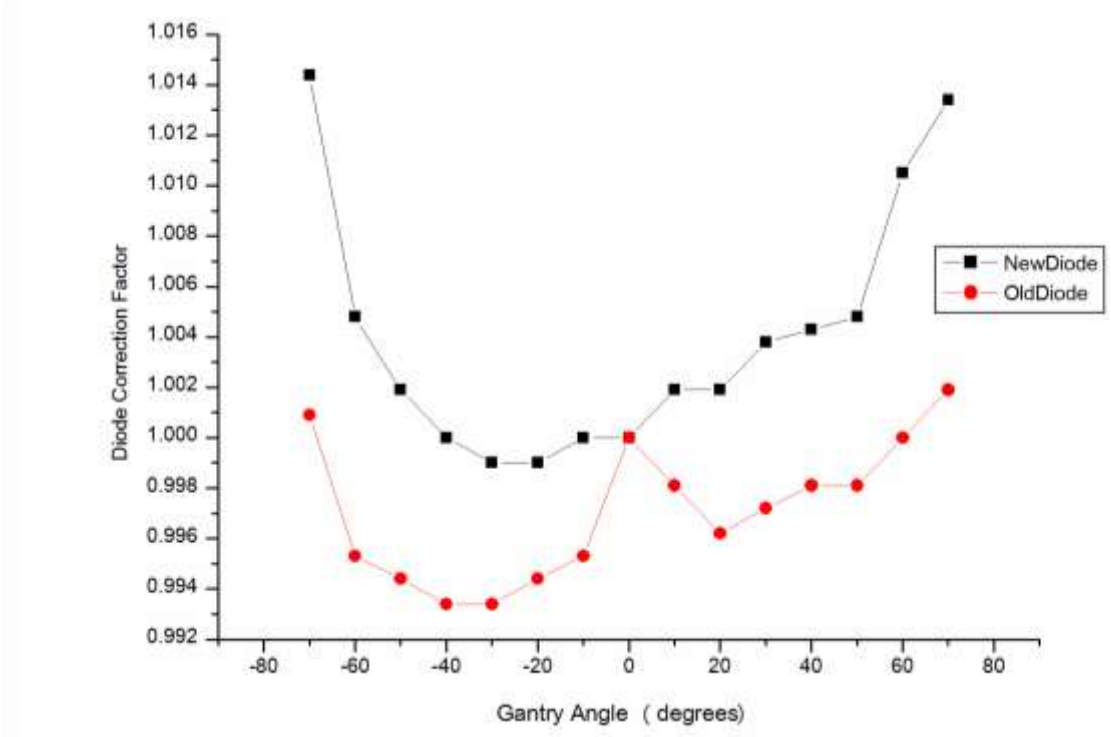

Figure 4.2: Diode correction factors as a function of gantry angle on a flat surface.

The Isorad diode used was cylindrical as shown in the figure 2.2. The schematic diagram shows that the silicon die is situated at the center (figure 2.2). It is natural to expect the dose response of the diode to be symmetrical about the 0^{o} gantry angle.

The measured results show that there is no symmetry in the plotted results as shown in figure 4.1 and 4.2. The difference in measured readings between the old and the new diodes curves is as a result of the sensitivity variation with accumulated dose in the old silicon diode.

Figure 4.2 shows the variation of the diode correction factors of the two diodes calculated using equation 2.15. Comparing figure 4.2 with that from the user's manual figure 2.6, there are similarities in the shape of the graphs. The diode correction factor graphs are normalised to the 0^{o} gantry angle.

Equation 4.5 is used to obtain the percentage deviation,

$$Percentage\ Deviation = \frac{Measured\ dose - Expected\ dose}{Expected\ dose} \times 100\% \qquad 4.5$$

It is noted that the diode correction factor for the old diode can have a deviation of about ±1.4% at most, whereas the new diode has the highest percentage deviation of the order of ±0.6%. This shows that the new diode gives a higher dose as illustrated in figure 4.1.

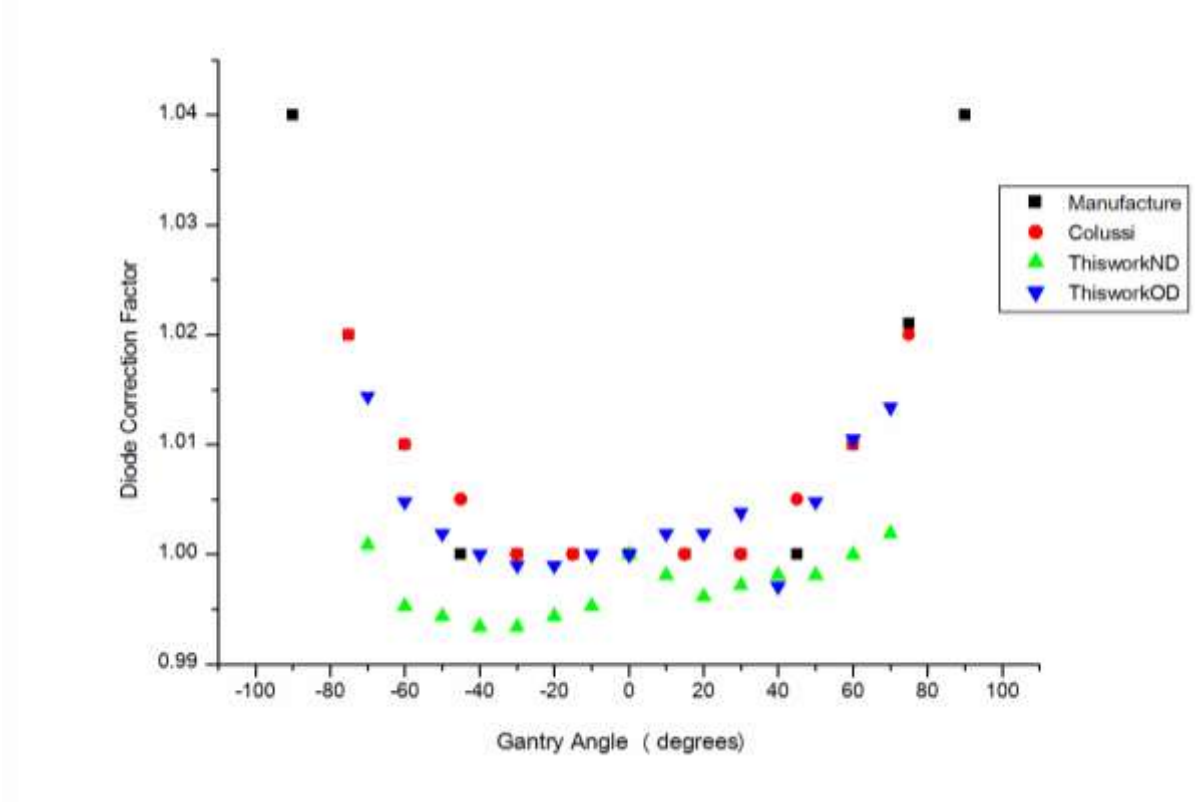

Figure 4.3: A comparison of diode correction factors of Isorad p-type diodes from three different authors varying the gantry angle.

Figure 4.3 shows that at ±90° gantry angle, the diode correction factor data from the manufacturer's manual deviates by about 4%, this is because of the range of angles included in their study (-90° to 90°). In the range of concern in this study (-70° to 70°) the percentage deviation is less than 2% in all cases.

The non-symmetry in the measured readings could be a result of the phantom and the independent diode positioning methods employed during the measurements.

The following subsection consists of results of angular dependence with the diode placed on the curved surface of the phantom.

Table 4.3: Results for diode correction factors and measured doses as a function of gantry angle on a curved surface.

Gantry Angle (°)	Measured Dose ND(cGy)	Measured Dose OD(cGy)	Correction Factor ND	Correction Factor OD	% deviation (ND) ±	%deviation (OD) ±
-50	106.0	106.6	1.0115	1.0329	1.15	3.29
-40	105.3	105.0	1.0048	1.0174	0.48	1.74
-30	105.3	104.2	1.0048	1.0097	0.48	0.97
-20	105.1	103.8	1.0029	1.0058	0.29	0.58
-10	105.1	103.3	1.0029	1.0010	0.29	0.10
0	104.8	103.2	1.0000	1.0000	0.00	0.00
10	104.2	103.2	0.9943	1.0000	0.57	0.00
20	104.0	103.0	0.9924	0.9981	0.76	0.19
30	104.0	103.1	0.9924	0.9990	0.76	0.10
40	103.7	103.0	0.9895	0.9981	1.05	0.19
50	103.8	102.8	0.9905	0.9961	0.95	0.39
60	104.2	102.6	0.9943	0.9942	0.57	0.58
70	104.2	103.3	0.9943	1.0010	0.57	0.10
80	104.1	103.3	0.9933	1.0010	0.67	0.10
90	103.9	103.1	0.9914	0.9990	0.86	0.10
100	-	103.0	-	0.9981	-	0.19
110	-	103.2	-	1.0000	-	0.00
120	-	103.7	-	1.0048	-	0.48

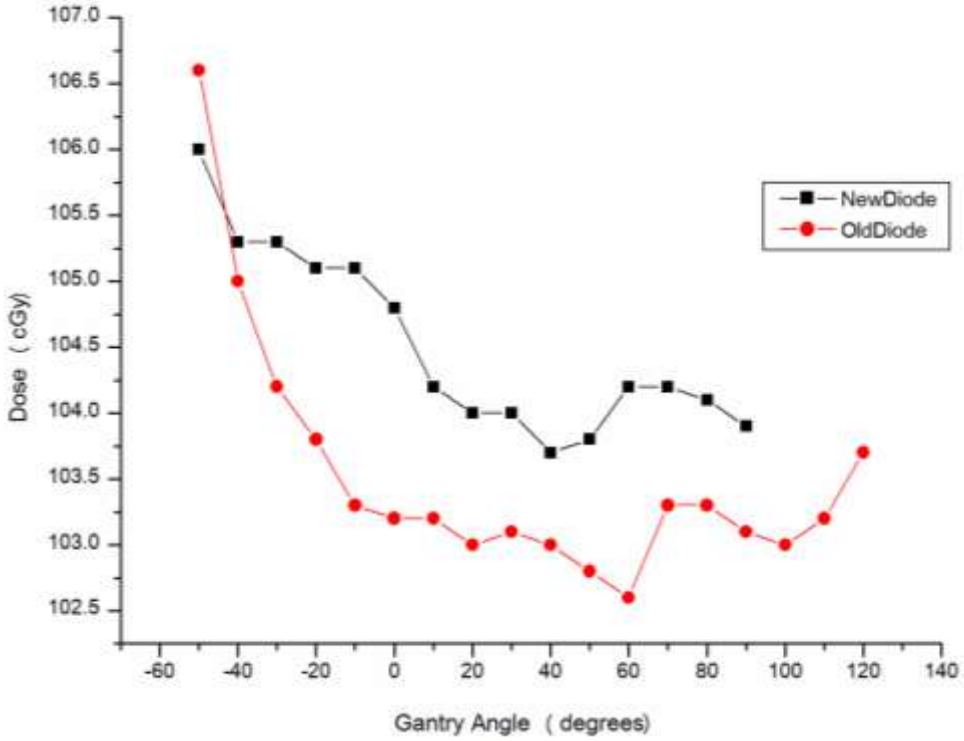

Figure 4.4: Variation of measured dose with gantry angle on a curved phantom surface.

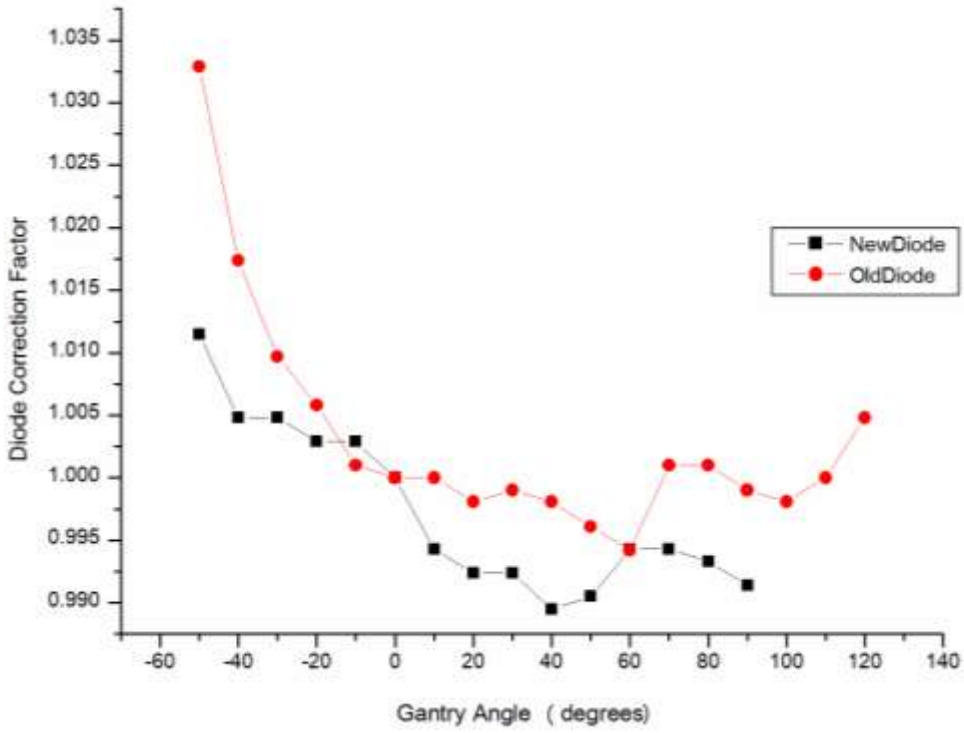

Figure 4.5: Diode correction factors as a function of gantry angle on curved surface.

When the diode is placed on the curved surface of the phantom the range of gantry angle used differ from those used during measurements on flat surfaces. The measured dose figure 4.4 decreases as the gantry is moved clockwise from -60° to 120°. The symmetry is completely lost for both diodes about the 0° gantry angle. The increase in dose between 60° and 70° is as a result of the different scatter contribution from the phantom, as the beam central axis is almost perpendicular to the curved phantom surface.

The highest percentage deviation calculated using equation 4.5 is approximately ±3.3% for the old diode in the range between -70° and 140°, whereas that of the new diode is approximately ±1.15% (figure 4.5). This emphasises the need to regularly recalibrate the diode even if the validation results are acceptable. The results from the experiment also show clearly the need to exercise care when dealing with curved surfaces.

The diode construction is such that the plane of the die is mounted normal to the cable axis and the die is surrounded with a cylindrical sleeve of build-up as shown in figure 2.2. The orientation of the die during measurements is approximately parallel to the beam axis.

Yorke *et al* [8] highlighted that cylindrical detectors have a small directional dependence which effectively changes by less than 2% for angles less than ±70°. This can be seen to be false for curved phantom surface measurements but true for flat phantom surface measurements.

4.4 Field size dependence

Table 4.4 shows the variation in response of the diodes with field size. A comparison of equivalent square field and rectangular field is also highlighted here.

Table 4.4: Diode correction factors for rectangular field size at a constant SSD of 100 cm

Actual Field Size (cm^2)	Correction factor (ND)	Correction factor (OD)	% deviation (ND) ±	% deviation (OD) ±
4x9	0.9754	0.9781	2.46	2.19
4x12	0.9819	0.9837	1.81	1.63
6x9	0.9773	0.979	2.27	2.10
6x9	0.9828	0.9828	1.72	1.72
7x10	0.9942	0.9961	0.58	0.39
8x13	1.0049	1.0059	0.49	0.59
10x10	1.0000	1.0000	0.00	0.00
8x20	1.0208	1.0219	2.08	2.19
10x15	1.0218	1.0239	2.18	2.39
15x20	1.0249	1.0260	2.49	2.60

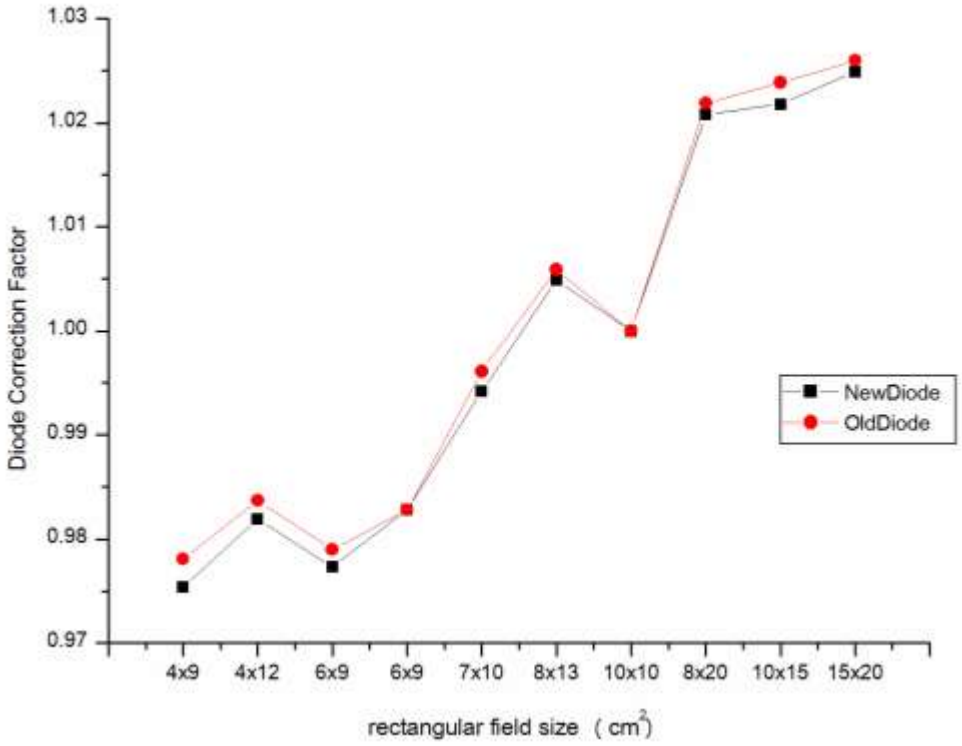

Figure 4.6: Diode correction factor variation with rectangular field sizes.

Table 4.5: Diode correction factors for equivalent square field at constant SSD.

Equivalent Square Field (cm^2)	Correction factor (ND)	Correction factor (OD)	% deviation (ND) ±	% deviation (OD) ±
5.5	0.9699	0.9735	3.01	2.65
6	0.9736	0.9762	2.64	2.38
6.9	0.9736	0.9772	2.64	2.28
7.2	0.9800	0.9809	2.00	1.91
8.2	0.9913	0.9923	0.87	0.77
9.9	1.0000	1.0010	0.00	0.10
10	1.0000	1.0000	0.00	0.00
11.4	1.0098	1.0128	0.98	1.28
12	1.0178	1.0199	1.78	1.99
17.1	1.0228	1.0250	2.28	2.50

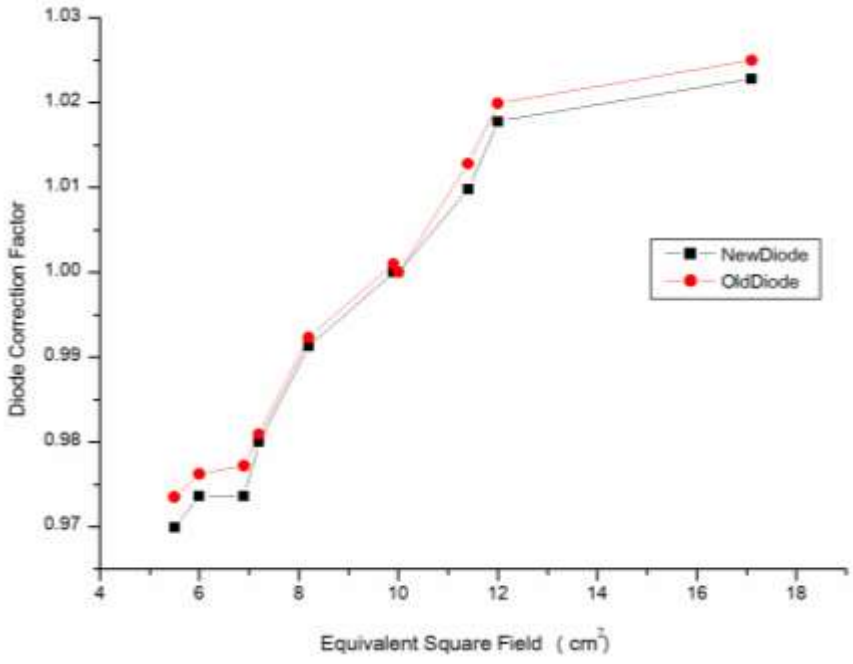

Figure 4.7: Diode correction factors variation with equivalent square field sizes.

Literature [4,8,10] predicts that the diode correction factors increase with increase in field size. A similar trend is observed in the measured results from both diodes which are complemented by results obtained by Colussi *et al* [23], Huang [15] and Yorke *et al* [8] figures 2.7, 2.8 and 2.9 respectively. The field size used in the investigation was limited to a 20 cm x 20 cm because it was the maximum size obtainable on the phantom.

A comparison of the results from the equivalent square field and the actual square field shows a close relationship between the two and it gives the validity of the equivalent square theory which was first proposed by Day [6]

$$Equivalent\ Square = \frac{4 \times Area}{Perimeter} = \frac{2ab}{a+b}, \qquad 4.6$$

where *a* and *b* are the length and width of the radiation field respectively.

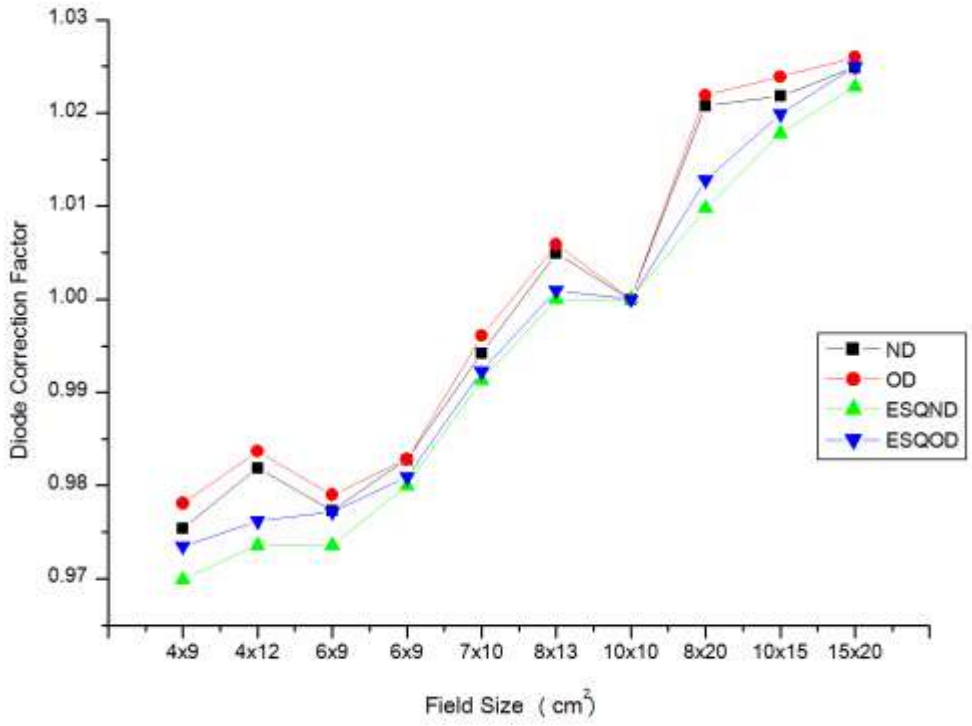

Figure 4.8: A comparison of the rectangular field size and the equivalent square field (ESQ) using diodes.

As the field size increases the diode correction factor approaches 2.5%. The trend and magnitude of the results are similar for both diodes.

4.5 SSD dependence

The response of the diode with different source to surface distance, SSD is highlighted in this section. The diode correction factors normalised to 100 cm is plotted for several field sizes.

Table 4.6: Results for diode correction factors as a function of SSD for different field sizes.

SSD (cm)	5 x 5 (ND)	5 x 5 (OD)	10 x 10 (ND)	10 x 10 (OD)	20 x 20 (ND)	20 x 20 (OD)
80	0.9493	0.9477	0.9389	0.9399	0.9400	0.9383
90	0.9630	0.9651	0.9782	0.9779	0.9795	0.9792
100	1.0000	1.0000	1.0000	1.0000	1.0000	1.0000
110	1.0057	1.0106	1.0088	1.0120	0.9901	0.9950
120	1.0230	1.0174	1.0269	1.0221	1.0070	1.0061

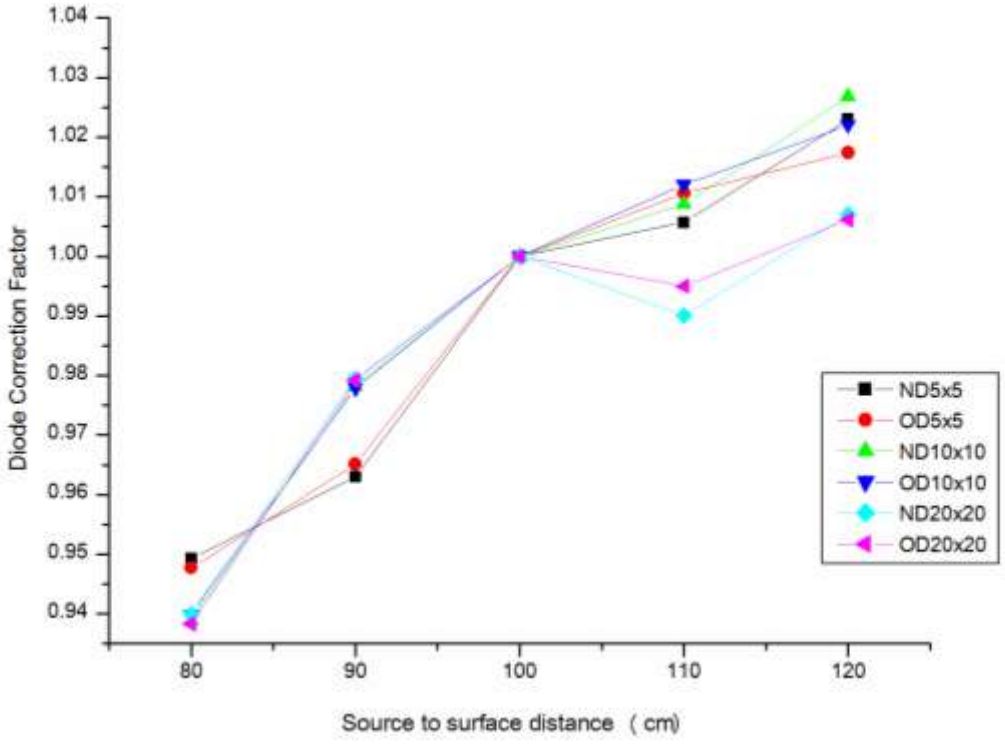

Figure 4.9: Diode correction factors as a function of SSD for 5, 10 and 20 cm^2 field sizes.

Figure 4.9 shows a graph of diode correction factor normalised at 100 cm SSD for 5, 10 and 20 cm^2 field sizes. The graph shows that the correction factors increases with increase in source to surface distance (SSD). This is explained by the increased number of contamination electrons which are able to reach the sensitive part of the diode, which can be attributed to the inverse square law.

The graph shows that the SSD dependency is not influenced by field sizes especially for the 5 cm x 5 cm and the 10 cm x 10 cm, for larger field sizes 20 cm x 20 cm and larger SSD 110 cm notable influence is perceived. At smaller SSD percentage deviation is about ±6%, this is explained by the increased dose per pulse at short SSDs.

4.6 Off-axis dependence

Table 4.7: Off-axis dose measurements and correction factors for flat surface.

Off axis distance (cm)	Measured Dose (OD) (cGy)	Measured Dose (ND) (cGy)	Correction factor Old diode	Correction factor New diode	% deviation (OD) ±	% deviation (ND) ±
-4	103.6	104.1	1.0010	1.0019	0.10	0.19
-3	104.2	106.1	0.9952	0.9830	0.48	1.70
-2	104.3	105.1	0.9942	0.9924	0.58	0.76
-1	104.4	104.6	0.9933	0.9971	0.67	0.29
0	103.7	104.3	1.0000	1.0000	0.00	0.00
1	102.6	103.3	1.0107	1.0097	1.07	0.97
2	103.3	103.8	1.0039	1.0048	0.39	0.48
3	103.9	103.7	0.9981	1.0058	0.19	0.58
4	102.7	103.2	1.0097	1.0107	0.97	1.07

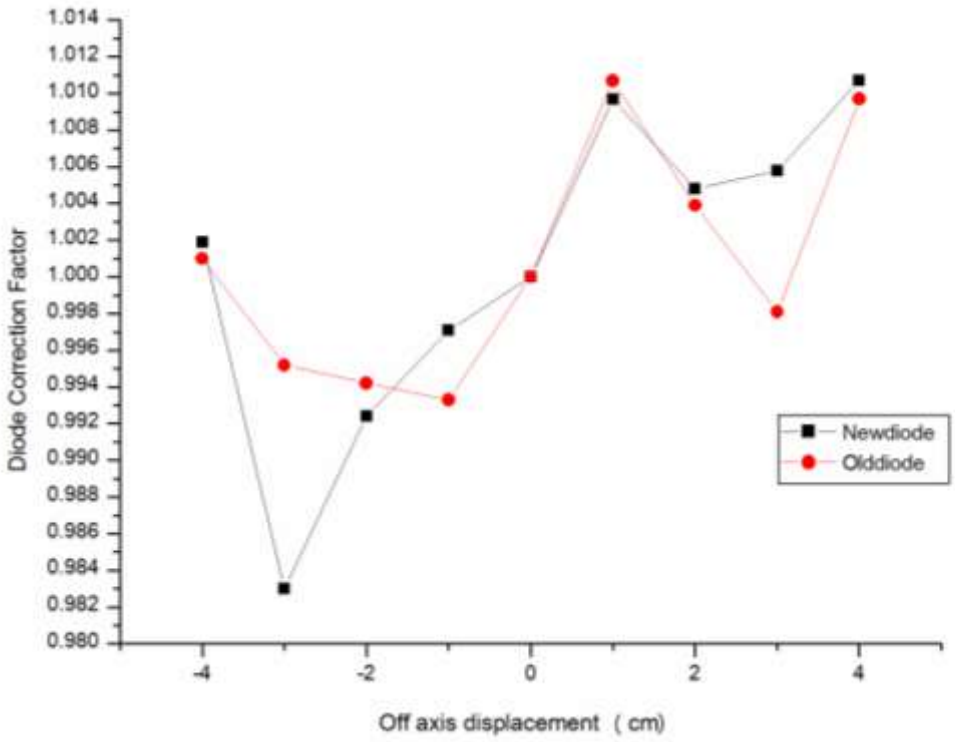

Figure 4.10: Diode correction factors for off-axis dependence on flat surface.

Table 4.7 and Table 4.8 give the tabulated results for off-axis dose measurements with the corresponding correction factors for flat surface and curved surface measurements.

Figure 4.10 show the variation of the diode correction factor with distance from the central axis of the beam. A comparison of figure 4.10 with the work of Herbert *et al* [20] figure 2.12 shows the difference in trend between the two graphs. These graphs whose results are obtained under slightly different conditions do not match.

The measured dose is expected to be flat (i.e. constant at 1.00) with deviation less than 1% towards the edge of the fields. The reason why the diode behaves as in figure 4.10 is because of different backscatter conditions and type of machine as explained in section 4.6.

Table 4.8: Results for the off-axis dose measurements and the diode correction factors on curved surface.

Distance off axis (cm)	Measured dose (OD) (cGy)	Measured dose (ND) (cGy)	Correction factor Old diode	Correction factor New diode	% deviation (OD) ±	% deviation (ND) ±
-4	108.9	110.4	0.9256	0.9266	7.44	7.34
-3	106.5	107.6	0.9465	0.9507	5.35	4.93
-2	105.2	106.5	0.9582	0.9606	4.18	3.94
-1	103.6	104.3	0.9730	0.9808	2.70	1.92
0	100.8	102.3	1.0000	1.0000	0.00	0.00
1	99.5	100.5	1.0131	1.0179	1.31	1.79
2	98.8	98.8	1.0202	1.0354	2.02	3.54
3	97.0	96.8	1.0392	1.0568	3.92	5.68
4	96.1	96.8	1.0489	1.0568	4.89	5.68

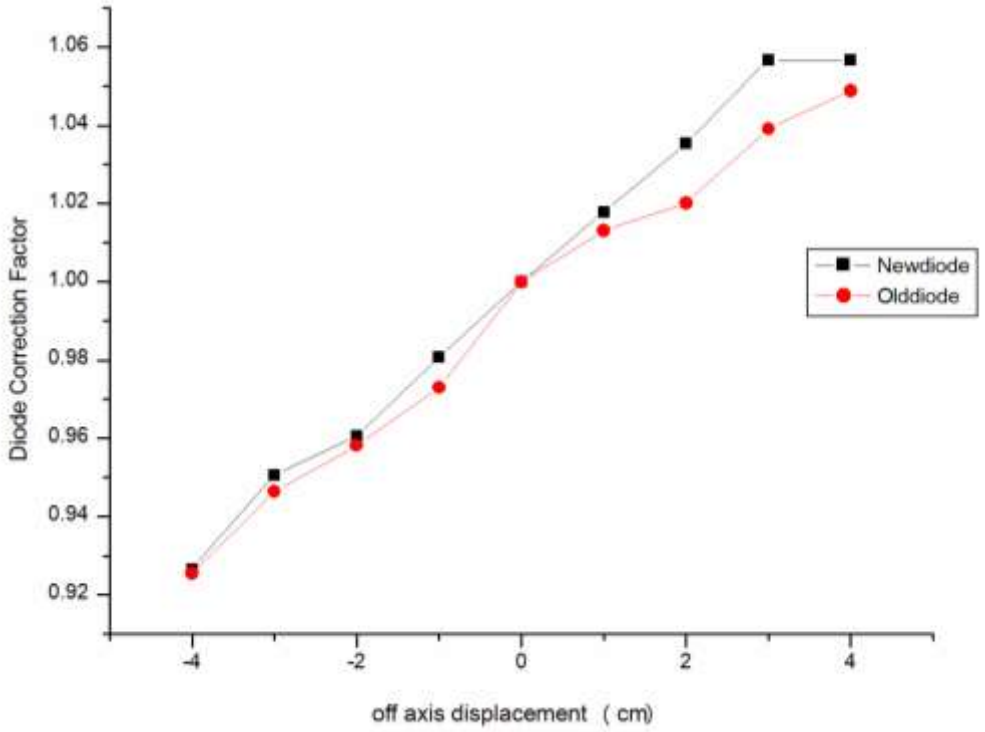

Figure 4.11: Diode correction factors as a function of off axis distance on curved surface.

Figure 4.11 represents the variation of diode correction factor as a function of distance from the central axis of the radiation beam for measurements done on curved surface. The trend of the diode correction factors in this respect is similar to that of the diode dependence with SSD. The values of the correction factors increases with distance from central axis, this is due to the change in dose rate detected by the die. The percentage deviation increases as we move away from the central axis in both directions the highest percentage deviation is approximately ±7.3%.

The variation of the diode correction factors as shown in figures 4.10 and 4.11 for curved and flat phantom surface measurements differ because:

i) for flat surface measurements, only the phantom and machine scatter contribute to the radiation reaching the die; and
ii) for curved surface measurements, in addition to the phantom and machine scatter, the dose rate dependence also contribute to the dose measured.

The shape of graph in figure 2.12 is influenced by the wedge present during measurements, which is another reason the two graphs are different in shape.

The result of figure 4.11 is similar to the results obtained by Huang, 2002 [15] figure 2.12 and the user's manual from the manufacturer [10].

4.7 Wedge angle dependence

The following section brings into perspective the influence of the use of beam modifiers such as physical wedges on diode measurements. Physical wedge angle dependence was investigated at constant SSD.

Table 4.9: Results for wedge angle dependence with varying field size.

Field size (cm^2)	15 Wedge (ND)	15 Wedge (OD)	30 Wedge (ND)	30 Wedge (OD)	45 Wedge (ND)	45 Wedge (OD)	60 Wedge (ND)	60 Wedge (OD)
5	0.9769	0.9714	1.2072	1.2136	0.9768	0.9789	0.9807	0.9834
8	0.9980	1.0000	0.9970	0.9981	1.0010	1.0000	1.0042	1.0054
10	1.0000	1.0000	1.0000	1.0000	1.0000	1.0000	1.0000	1.0000
12	1.0040	1.0048	1.0000	1.0000	1.0010	1.0009	1.0010	1.0027
15	1.0060	1.0067	0.9970	0.9963	0.9990	0.9991	0.9979	0.9991
20	1.0040	1.0038	0.9970	1.0000	0.9959	0.9963	-	-

Table 4.10: Measured diode dose as a function of field size and wedge angle at constant SSD, the measured doses are in cGy.

Field size (cm^2)	15 Wedge (ND)	15 Wedge (OD)	30 Wedge (N D)	30 Wedge (OD)	45 Wedge (ND)	45 Wedge (OD)	60 Wedge (ND)	60 Wedge (OD)
5	103.8	108.4	83.0	88.0	99.2	109.1	98.3	114.4
8	101.6	105.3	100.5	107.0	96.8	106.8	96.0	111.9
10	101.4	105.3	100.2	106.8	96.9	106.8	96.4	112.5
12	101.0	104.8	100.2	106.8	96.8	106.7	96.3	112.2
15	100.8	104.6	100.5	107.2	97.0	106.9	96.6	112.6
20	101.0	104.9	100.5	106.8	97.3	107.2	-	-

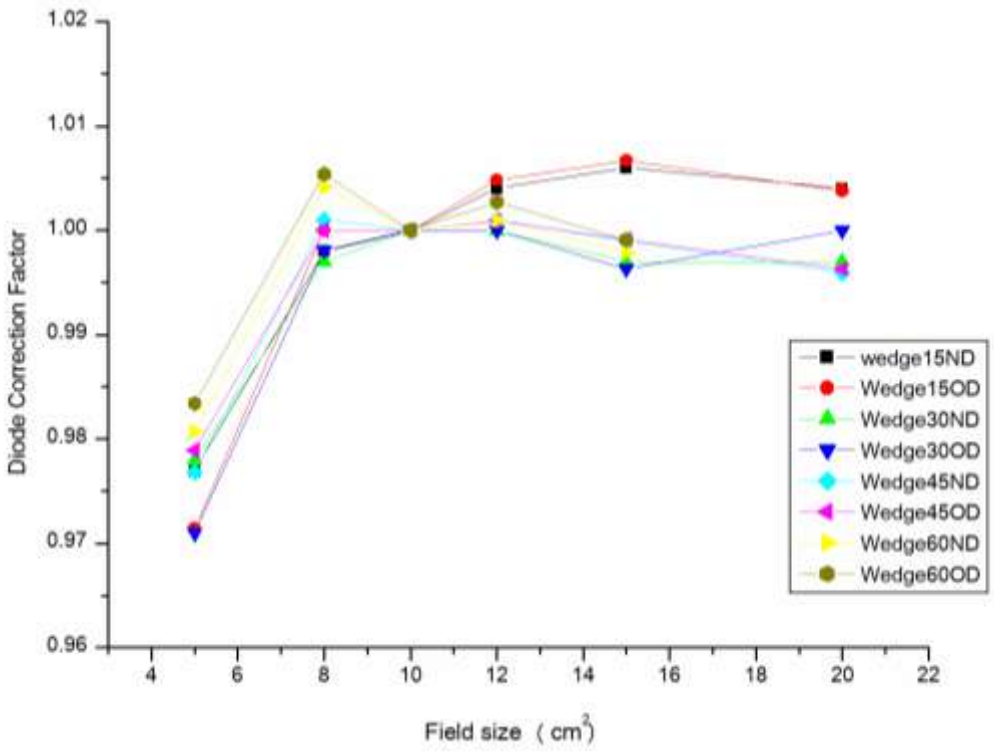

Figure 4.12: Diode correction factors as a function of wedge angle and field size.

The graph of figure 4.12 indicate a percentage deviation of ±0.5 % in the diode correction factor, for field sizes between 8 cm^2 and 12 cm^2 for all physical wedges used. The diode correction factor is close to 1.00 for this range of field sizes. However the graph show that the correction factor decreases with increase in physical wedge angle, the percentage deviation is close to 1% for 20 x 20 cm^2 field size.

Scatter contribution affects the diode correction factor for field sizes less than 8 cm^2, hence the diode tends to increase the measured dose.

Chapter 5

RECOMMENDATIONS AND CONCLUSIONS

6.1 Introduction

This chapter presents a short summary of experimental findings, conclusions and recommendations for future work. The summary and conclusion gives answers to the objectives stated in chapter 1. The chapter ends with recommendations for improving these results and for future work.

6.2 Summary of findings

A summary of the findings from the experiments is given below:

i. Silicon semiconductor diodes can be used on any surface either curved or flat to measure radiation;
ii. Silicon diode placement is very important to obtain accurate results;
iii. The diode correction factors assist to set clinically achievable tolerance or action levels;
iv. Silicon diode behaves differently on curved surface and flat surface measurements;
v. The diode correction factor behaved differently under each parameter, which makes it difficult to base on the accuracy of the diode as a standard;
vi. The deviation between the measured dose and the expected dose is acceptable clinically in most cases i.e. less than 7%;
vii. Larger percentage deviations are observed on curved surface measurements than on flat surface measurements;
viii. Small field sizes less than 8 cm^2 also contribute to the larger deviation in measurement results;
ix. Diodes can be used as an independent method to verify the equivalent square field theory; and
x. It is possible to use local resources to build a phantom which has similar properties to that of a patient.

6.3 Conclusions

Two p-type silicon semiconductor diodes were characterised for use in radiation treatments.

The response of the diodes was investigated for a number of parameters.

The response was obtained by altering the SSD, field size, angle of incidence, off axis displacement and wedges.

The following diode correction factors were obtained during the investigations:

i. For equivalent square field, the range for diode correction factors is between 0.970 and 1.030;
ii. For the rectangular field, the range for diode correction factors is between 0.975 and 1.030;
iii. For SSD, the range for diode correction factors is between 0.940 and 1.030,
iv. For angular dependence (curved surface measurements), the range for diode correction factors is between 0.990 and 1.035;
v. For angular dependence (flat surface measurements), the range for diode correction factors is between 0.994 and 1.016;
vi. For wedge angle, the range for diode correction factors is between 0.970 and 1.010;
vii. For off axis (curved surface measurements), the range for diode correction factors is between 0.930 and 1.060; and
viii. For off axis (flat surface measurements), the range for diode correction factors is between 0.982 and 1.012.

From the above diode correction factors the highest percentage deviation is within ±7%, which can be taken as the tolerance or action level for the measured values.

Besides the difference in calibration factors of the two diodes (old and new), the correction factors showed similar trends.

6.4 Recommendations

The following are my recommendations:

The manufactured phantom can be incorporated into the departmental protocol to test any new treatment technique involving the thorax region of the body. The diodes can be applied to verify the dose at a point before the actual treatment.

Different types of diodes should be investigated so that the best diode with the best response is chosen for a particular measurement procedure.

The response of the diodes in high energy electron beams should be investigated in future work. A program to quickly calculate the final dose should be included since a lot of correction factors are involved during measurements.

The currently adopted diode calibration procedure employs an ionisation chamber which has some uncertainties which are transferred to the diode itself. It is proposed that the use of theoretical doses obtained from manual calculations using already available data tables as the reference dose should be adopted.

To improve the results (for example extended SSD and off axis measurements) positional measurements should be read from the machine rather than using the optical distance indicator.

It is recommended that a controlled experiment should be designed to investigate the effect of the nature of the interface, because the phantom is expected to have different scattering and absorption capabilities.

Reference

1 P. Andreo, D.T. Burns, K. Hohlfeld, M.S. Huq, T.Kanai, F. Laitano, V.G Smythe, S. Vynckier, *Absorbed dose determination in external beam radiotherapy, TRS 398,* IAEA Vienna(2000)

2 P. Mangili, C. Fiorino, A. Rosso, G. M. Cattaneo, *Quality assurance by systematic in vivo dosimetry: results on a large cohort of patients*, Radiotherapy and Oncology **56**, Elseveir, 85-95 (2000)

3 A. Strojnik, *In-vivo dosimetry with diodes in radiotherapy patients treated with four field box technique*, IFMBE proceedings **Vol 16,** (2007)

4 D. P. Huyskens, R. Bogaerts, J. Verstraete, M. Lööf, H. Nyström, C. Fiorino, S. Broggi, N. Jornet, M. Ribas, D. I. Thwaites, *Practical Guidelines for implementation of in-vivo dosimetry with diodes in external radiotherapy with photon beams (entrance dose)*, ESTRO (2001)

5 ICRU, *Determination of absorbed dose in a patient irradiated by beams of x or gamma rays in radiotherapy procedures Report 24*, ICRU, Bethesda MD (1976)

6 F. M. Khan, *The physics of radiation therapy, 3rd ed*, Lippincott William and Wilkins, Baltimore, (1994)

7 A. Dutreix, *When and how can we improve precision in radiotherapy?* Oncology **2** 275–292 (1984)

8 E. Yorke (Chair), R. Alecu, L. Ding, D. Fontenla, A. Kalend, D. Kaurin, M. E. Masterson-McGary, G. Marinello, T. Matzen, A. Saini, J. Shi, W. Simon, T.C. Zhu, X. R. Zhu, *Diode in-vivo dosimetry for patients receiving external beam radiation therapy*, AAPM report No **87** Medical Physics Publishing, Madison, (2005)

9 R. J. Meiler, M.B. Podgorsak, *Characterisation of the response of commercial diodes detectors used for in-vivo dosimetry, Medical Dosimetry* **Vol 22**, Elsevier, 31-37(1997)

10 User's Guide, *ISORAD detector*, Sun Nuclear Corporation (2005)

11 M. Voordeckers, H. Goossens, J. Rutten, W. Van den Bogaert. *The implementation of in-vivo dosimetry in a small radiotherapy department*, Radiotherapy and Oncology **47**, 45-48 (1998)

12 D.P. Rontenla, R. Yaparpalvi, C. Chui, E.Briot. *The use of diode dosimetry in quality improvement of patient care in radiation therapy, Medical Dosimetry* **Vol 21**, Elsevier, 235-241 (1996)

13 G. Rickener, E. Grusell , *General specification for silicon semiconductor for use in radiation dosimetry*, Phys. Med.Biol, **Vol 32,** 1109-1117(1987)

14 H. Johns and J. Cunnigham, *The physics of radiology*, 4th ed. (Charles Thomas, 1983).

15 K. Huang , *Characterisation of an in-vivo diode dosimetry system for clinical use*, White paper, Louisiana State University, (2002)

16 A. S. Saini, *In-vivo radiation diode dosimetry for therapeutic photon beams*, White paper, University of South Florida, (2007)

17 S.M. Sze, *Physics of semiconductor devices*, Wiley-Interscience, (1969)

18 G. J. Kutcher, L. Coia, M. Gillin, W. F. Hanson, S. Leibel, R. J. Morton, J. R. Palta, J. A. Purdy, L. E. Reinstein, G. K. Svensson, M. Weller, and L. Wingfield, *Comprehensive QA for Radiation Oncology*, AAPM Radiation Therapy Committee Task Group 40, AAPM Report No. 46, American Association of Physicists in Medicine (American Institute of Physics, New York) (1994)

19 E. P. Podgorsak, *Radiation Oncology Physics: A handbook for teachers and students*, Vienna, IAEA, (2005)

20 C.E. Herbert, M.A. Erbert and J. Joseph, *Feasible measurements errors when undertaking in-vivo dosimetry during external beam radiotherapy of the breast*, Medical Dosimetry, Vol 28, Elsevier, 45-48(2003)

21 S.Tavernier (eds), *Radiation detectors for medical applications*, Springer, 111-147 (2006)

22 A. Ridanzio, F. Greco, A. Marneli, L. Azario, M. Balducci, M.A. Gambacorta, V. Frascino, S.Cilla, D.Sabatino and A. Piermattei, *Breast in-vivo dosimetry by EPID*, Journal of Applied Clinical Medical Physics, Vol 11, Number 4 (2010)

23 V.C. Colussi, A. Poeddar, T.J. Kinsella and C.H. Sibata, *In-vivo dosimetry using a single diode for megavoltage photon beam radiotherapy: Implementation and response characterisation*, Journal of Applied Clinical Medical Physics, Vol 2, Number 2, (2001)

24 E.J. Bloemen-van Gurp, W.F.J. du Bios, P.A. Visser, I. Bruinuis, D.Jalink, J. Hermans and P. Lambin, *Clinical dosimetry with MOSFET dosimeters to determine the dose along the field junction in a split beam technique*, Radiotherapy and Oncology 67, 351-357 (2003)

25 E.J. Bloemen-van Gurp, A.W.H. Minken, B.J. Mijnheer, C.J.G. Dehing-Oberye and P. Lambin, *Clinical implementation of MOSFET detectors for dosimetry in electron beams*, Radiotherapy and Oncology 80, 288-298 (2006)

Appendix 1

GLOSSARY OF TERMS

AAPM	American Association of Physicists in Medicine
cGy	centiGray
d_{max}	Depth of maximum dose
D_{max}	Maximum dose
ESQ	Equivalent square
Gy	Gray
IAEA	International Atomic Energy Agency
Linac	Linear Accelerator
MeV	Mega electron Volt
MOSFET	Metal oxide semiconductor field effect transistor
MU	Monitor Unit
MV	MegaVolt
ND	New diode
OD	Old diode
PDD	Percentage depth dose
R(100)	diode reading at 100 cm
rf	radio frequency
SAD	source to axis distance
SSD	Source to surface distance
TG	Technical group
TLD	Thermoluminescence dosimeter
TRS	Technical report series

Appendix II

Calibration protocol "IAEA TRS 277" for all energies on the Varian 2100C

II.1 Preamble

As part of the daily running of the 2100C, absolute dose check on all photon and electron energies must be performed. Obviously, the energy checked must be the one that is to be used during the day clinically. The method of calculating dose is according to the IAEA protocol TRS 277 which is based on absorbed dose to water.

Apparatus

PTW Unidos electrometer

PTW ion chamber W30012

PMMA phantom

Method

i. Plug the ionisation chamber before switching the PTW Unidos on. Allow the chamber to warm up for 5 minutes.

ii. Correct for temperature and pressure, $\rho_{tr} = \left(\frac{1013}{P} \times \frac{273+T}{293}\right)$ II.1

iii. Build a pile of solid water (PMMA), 15 cm deep.

iv. Position the layer on top of the 15 cm PMMA and align with cross hairs

v. To calibrate a particular energy, add an appropriate amount of PMMA, which is obtained from the table II.1.

vi. Ensure that the top stack is exactly at SSD 100 cm. Set the field size to 10 cm x 10 cm for photons and for electrons insert a 10 cm x 10 cm applicator.

vii. Give three irradiations of 200MU each, take down the reading and calculate mean reading M_Q

viii. $Calibration\ factor = M_Q \times P_{tr} \times RW3\ factor \times N_D S_{w,air} P_u$(cGy.MU^{-1}) II.2

Table II.1: Correction factors for calibration according to TRS 277

Beam Energy	**Depth of RW3 (cm)**	**PDD (depth)**	**RW3 factor**	$N_D S_{w,air} P_u$
10X	10 5	73.9 (10 cm) 92.6 (5 cm)	1.016	0.974
6X	10 5	66.8 (10 cm) 86.49 (5 cm)	1.009	0.986
20e	4.2	99	1.007	0.884
16e	3.6	100	1.013	0.893
12e	3.1	100	1.020	0.907
9e	2.3	100	1.023	0.914
6e	1.5	100	1.022	0.923

Action levels

If the reading deviates from 1cGy.MU^{-1} by more than 3 %, then the dosimetry levels for that energy may need to be adjusted. The weekly protocol using measurements in water should be performed as soon as possible.

If the reading deviates by more than 10% then this energy should not be used until a full evaluation is performed.